nature climate change

Supplementary information https://doi.org/10.1038/s41558-025-02303-3

Dual impact of global urban overheating on mortality

In the format provided by the authors and unedited

Table-of-contents

A. Supplementary Notes

<u>Note S1</u>: *Impacts of cooling strategies on temperature-related mortality in the future*

We analyzed the annual net impacts of several urban cooling strategies on temperature-related mortality around 2050 under a moderate emission pathway (SSP2-4.5; Supplementary Fig. S9). The cooling strategies involve increasing urban vegetation coverage and surface albedo by 4% to 40% from baseline levels, spanning five regulatory intensities from low to high by considering varying population density and albedo levels across cities (refer to Methods). Our evaluations reveal that globally, increasing urban vegetation fraction could reduce future heat-related mortality by 0.2% to 1.1% across the spectrum of regulatory intensities, but increase future cold-related mortality by 1.1% to 5.7% (Supplementary Fig. S10). Similarly, enhancing albedo can reduce heat-related mortality by 1.1% to 5.4% but increase cold-related mortality by 5.7% to 29.9% under low to high regulation intensity (Supplementary Fig. S10). We observe that, by implementing these two cooling strategies, the global mean increase in cold-related mortality consistently surpasses the decrease in heat-related mortality (Supplementary Fig. S9). The global mean detrimental annual net impact can sextuple when the cooling intervention intensifies (Supplementary Fig. S9), even after factoring future global warming.

Seasonal adjustment of surface albedo (e.g., by repainting roofs and pavements) is more feasible than adding vegetation over urban areas[1]. To mitigate the adverse impacts of increasing surface albedo on cold days while preserving its benefits on heat days, we modified the original cooling strategy with a constant surface into a season-dependent one. This season-dependent albedo strategy involves increasing surface albedo on heat days, while reducing it by 8%, 6%, and 4% from baseline levels on cold days for cities with low, medium, and high albedo classes, respectively (see Methods). This combined 'black-white' roof strategy is engineeringly feasible, for instance, by using specific materials that change with the solar incident angle or surface temperature[2-4] or through repainting roofs and pavements bi-annually[5]. Our evaluations indicate that the use of a constant strategy is beneficial in most low-latitude cities while detrimental in middle- and high-latitude cities in the context of future climate change (Supplementary Fig. S9a & c). Globally, the implementation of constant albedo/vegetation cooling strategies at low regulatory intensity results in a net increase of 5.6% in temperature-related mortality, rising to 29.0 % under high regulatory intensity (Supplementary Fig. S9f). Nevertheless, the season-dependent strategy reduces the adverse effects of the constant strategy on cold-related mortality, yielding annual benefits (Supplementary Fig. S9b & d). As albedo regulation intensifies, this season-dependent approach not only mitigates but reverses the adverse effect (Supplementary Fig. S9e). Overall, the temperature-related mortality reduction ranges from 2.2% to 11.1% (Supplementary Fig. S9g). The net mitigation can increase from 2.2% to 6.5% under high vegetation regulatory intensity, from 5.8% to 10.2% under low regulation, and from 6.7% to 11.1% with no regulation (Supplementary Fig. S9g).

<u>Note S2</u>: *Accuracy assessment of the modelled MMT and mortality estimates at different temperature percentiles for global cities*

We established a statistical mortality-temperature (M-T) relationships by training random forest (RF) models for approximately 700 cities worldwide. We then used these trained RF models to estimate the minimum mortality temperature (MMT) and mortality at four temperature percentiles (i.e., >5%, 5%-MMT, MMT-95%, and >95%) for 3,000-plus cities worldwide (refer to Methods). We used 80% of the data for training and the rest 20% for validation. The correlation (*r*) for the MMT is 0.91, and the mean absolute error (MAE) is 0.97 °C; the mean *r* for the mortality is 0.81, and the associated MAE is around 0.12 (Supplementary Fig. S17). To ensure the generalizability and accuracy of the RF model, the random training and validation splits were repeated 100 times[6]. The *r* and MAE of each split are shown in Supplementary Fig. S18. Our assessments show that the trained RF model possesses acceptable accuracies, indicating good model generalizability and applicability. For all splits, the mean r of the MMT is 0.90, and the mean MAE is 1.0 °C. The mean *r* of the mortality at different temperature percentiles is 0.79, and the mean MAE is 0.33 (Supplementary Fig. S18).

<u>Note S3</u>: *Sensitivity analysis of modeling scheme on mortality assessments across global cities*

Our study extrapolated findings from approximately 700 cities, unevenly distributed worldwide, to over 3,000 cities globally by dividing the M-T curve into four subdivisions. Concerns may arise that such extrapolation and division scheme of temperature percentiles could introduce uncertainties, potentially skewing the assessment of the dual impacts of the UHI effect on temperature-related mortality. To address these concerns, we conducted a sensitivity analysis to evaluate the robustness of our results concerning (1) the distribution of the city sample and (2) the division scheme of the temperature percentile.

Firstly, we adjusted the training sample dataset to further assess model sensitivity to uneven sample distribution and its impact on our primary findings. Our original model mainly incorporated city samples from two studies – those by Gasparrini et al.[7] and Kephart et al.[8], totaling approximately 700 cities (labeled *Dataset 1*). To test model sensitivity to sample distribution, we deliberately designed a comparison modeling experiment, which involves only city samples from Gasparrini et al.[7], totaling approximately 380 cities (labeled *Dataset 2*). When compared with *Dataset 2*, with cities sampled mostly in the Global North, *Dataset 1* encompasses a more extensive geographical coverage, incorporating a large number of cities in Latin America. This comparison experiment enabled us to evaluate model sensitivity to uneven sample distribution (e.g., in regions with substantial data gaps such as Global South cities) and their impact on the major findings.

Our sensitivity analysis demonstrates a high degree of consistency between the evaluations based on *Datasets 1 & 2*, both in terms of spatial distribution and specific values. To be specific, estimates derived from *Dataset 2* exhibit good alignment with those derived from *Dataset 1*, indicating UHI predominantly increases heat-related mortality and reduces cold-related mortality and that UHI has a beneficial net impact on the majority of global cities (Fig. S19a). Numerically, results from *Dataset 2* shows that UHI contributes an additional 10.4% increase to heat-related mortality and mitigates 47.0% of cold-related mortality on average (Fig. S19c-f). These values are comparable to the 11.7% increase and 51.5% mitigation estimated using *Dataset 1* (Fig. 1). The average beneficial impact of UHI is approximately 4.5 and 4.4 times higher than the detrimental impact based on *Datasets 1* and *2*, respectively, again suggesting a high consistency. These assessments suggest that our model exhibits low sensitivity to the less sampling in some continents (or uneven distribution of city samples), and consequently, our major findings remain generalizable.

Secondly, we conducted an additional analysis to explore the sensitivity of our results to the temperature percentile division scheme. Beyond the four-division scheme used in the primary analysis, we extended our tests to include an eight-division scheme, utilizing mortality data from over 380 cities[7] with the same modeling methodology. The results show strong spatial concordance between the UHI-induced impact derived from the eight-division and four-division scenarios. Notably, the majority of cities worldwide exhibited a net decrease in temperature-related mortality due to the UHI effect under both schemes (Fig. S19a, g). While minor variations in the intensity of the UHI-induced impact exist between the two division schemes, the spatial patterns observed using the eight-division scheme align closely with those derived from the four-division scheme. Importantly, these minor variations do not alter our primary findings (Fig. S19b, h). This additional analysis thus supports the robustness of our initial division scheme, indicating that it does not compromise our conclusions regarding the dual impacts of UHI effect on temperature-related mortality at both global and regional scales. These findings further bolster the validity of our study, suggesting that our conclusions remain reliable even when different division schemes are applied.

<u>Note S4</u>: *Potential impacts of model bias on mortality assessment for global cities*

We undertook a more detailed examination of the specific influence of model bias on our results. Specifically, we introduced the bias into the calculations of the impacts of the UHI effect and cooling strategies on temperature-related mortality. The potential impact of model bias on results was assessed by comparing these estimates with the original results.

Our examination demonstrates that the model bias has a slight impact on the impacts of the UHI effect and cooling strategies on temperature-related mortality. Nevertheless, the primary conclusions regarding the net effects of these strategies remain mostly consistent (Fig. S20). When modeling bias is added, the UHI effect has a negative impact of 14.8% on heat-related mortality and a mitigating effect of 65.5% on cold-related mortality for global cities (Fig. S20a). These values are slightly higher than the original results, which indicate a negative effect of 11.7% and a favorable effect of 51.5%. Overall, the mitigating effect of the UHI on cold-related mortality in global cities is 4.4 times greater than its negative impact on heat-related mortality, consistent with the original ratio (Fig. S20). With regard to cooling strategies, when bias is considered, the albedo and vegetation strategies can mitigate heat-related mortality by 7.2% and 1.6%, respectively, while simultaneously exacerbating cold-related mortality by 41.3% and 8.4%, respectively (Fig. S20b, c). In addition, the detrimental impact of albedo and vegetation strategies on cold-related mortality in global cities is 5.7 and 5.2 times their beneficial impact on heat-related mortality, respectively. These values are in close alignment with the original results, i.e., 5.6 and 5.1 times (Fig. S20). We acknowledge that model bias does affect the results, yet it does not substantially affect the major findings.

<u>Note S5</u>: *Cross-validation for the cities in Africa and South Asia*

We recognize the challenges posed by the scarcity of city samples in certain regions, which raises concerns about model accuracy. To assess model performance in regions with sample deficiencies, we resorted to additional data on temperature-mortality risk for selected cities in Africa and Asia. Through an extensive literature search, we additionally gathered data from 49 city samples, including 43 cities in South Africa[9], four in the Philippines[10], one in India[11], and one in Vietnam[10]. These samples provide temperature-mortality risk curves, which were used to validate our model. It is important to note that these 49 cities were excluded from the training process and served solely as validation samples.

Our validation indicates that the model achieves acceptable accuracy for cold-related mortality risk in these African and Asian cities (Fig. S21). Specifically, the discrepancies between the modeled and reference risk curves for cold-related mortality are primarily between –0.002 and 0.001 (Fig. S21a), with a mean discrepancy of only 0.0003, indicating a relatively robust modeling capacity. In terms of heat-related mortality risk, our evaluation shows that the model exhibits a slightly higher bias (Fig. S21d), with the difference falling between –0.04 and 0.04 (Fig. S21b), and a mean difference of around 0.02. The slightly lower accuracy in terms of heat-related mortality may be attributed to (1) the relatively higher intensity of heat-related risk and (2) the inherent modeling bias. To be specific, the model exhibits a slight underestimation of heat-related mortality risk for cities in the Philippines, Vietnam, and India, while a slight overestimation for South African cities.

In the majority of cities located in South Africa, the UHI effect was observed to typically exert a net beneficial influence. Therefore, the overestimation of heat-related mortality risk in these South African cities indicates a slight underestimation of the overall net benefits. Conversely, for the cities in the Philippines, Vietnam, and India where the UHI effect has a net detrimental impact, the underestimation of heat-related mortality risk implies a slight underestimation of the overall net detriments. These evaluations suggest that although biases exist, the major conclusions regarding the net impact of the UHI on temperature-related mortality across global cities remains valid.

<u>Note S6:</u> ***Robustness and validity of UHI-induced net mortality reduction in global cities***

Our investigation presents a comprehensive analysis of the dual impacts of the UHI effect and commonly employed cooling strategies on temperature-related mortality, spanning current and future scenarios across over 3,000 cities worldwide (Figs. 2 to 3 & Fig. S9). Our findings underscore the conventionally-acknowledged harmful impact of the UHI effect on temperature-related mortality in most low-latitude cities (such as Jakarta) and a few mid-latitude cities (Fig. 2). However, a markedly larger proportion of global cities (77.0%) experience a reduction in temperature-related mortality due to the UHI effect (Fig. 2). Globally, UHI-induced decrease in cold-related mortality outweighs the increase in heat-related mortality by approximately 4.4 times. Furthermore, the common vegetation and albedo cooling strategies could exhibit a net detrimental annual effect on global temperature-related mortality. While this finding may appear surprising, it is scientifically plausible given that these cooling strategies disproportionately exacerbate cold-related mortality compared to heat-related mortality in most cities. This can be attributable to the extended duration of cold-related risks within an annual cycle, where the global mean MMP is 77.9% (Supplementary Fig. S2). Traditional views often highlight the negative impacts of the UHI effect and the positive effects of cooling strategies; however, our research emphasizes the dual nature of the UHI effect and the associated cooling strategies on global temperature-related mortality.

Our assessments demonstrate the feasibility of the data-driven approach employed to establish mortality-temperature (M-T) relationships tailored to individual cities, achieving an acceptable level of accuracy (Supplementary Note S2). Moreover, our sensitivity analysis indicates that biases in the model exert only a minor influence on the assessment of UHI-induced annual net mortality (Supplementary Fig. S20), affirming the robustness of our core conclusions (Supplementary Note S4). Concerns may arise among practitioners regarding the validity of extrapolating global city-specific mortality-temperature (M-T) associations from a dataset with limited and unevenly distributed city samples (i.e., ~700 cities; see Methods). We acknowledge the inherent uncertainties associated with this approach. Nonetheless, our evaluations confirm that employing the random forest model alongside temperature-related data from around 700 cities produces reliable outcomes (Supplementary Note S3), despite the dataset's limited geographic representation, particularly in regions of the Global South (Supplementary Note S5). Another potential concern may be whether dividing the M-T association curve into four distinct ranges introduces uncertainties that could potentially skew the findings. Our further analysis shows that although some variability in the M-T association might arise from this division, the four-range partitioning strategy does not compromise the assessment of the dual impacts of the UHI effect on global mortality (Supplementary Note S3 & Fig. S9).

Numerous investigations on M-T associations have consistently highlighted a marked distinction, showing that mortality during cold seasons exceeds that during hot seasons by a factor of five to twenty in most urban settings[7,8,12]. Consequently, it is anticipated that the heightened warmth attributed to the UHI effect in most cities (with a relative warmth of approximately 1.0 K) would lead to a notably greater reduction in cold- than in heat-related mortality. Recent observational data, encompassing the past two decades and reflecting substantial warming akin to the relative warmth attributed to the UHI effect, indicate a substantial prevalence of cold-related over heat-related mortality[12]. Projections concerning temperature-related mortality also affirm that, even under high-emission scenarios with temperature increases during both hot and cold periods, heat-related mortality is projected to remain considerably lower than cold-related in most cities worldwide until 2050[13,14]. This phenomenon can be attributed to two key aspects: (1) the M-T curve displays an extended tail (i.e., the MMP often considerably exceeds 50%) at lower temperature percentiles, as opposed to higher percentiles, in most cities (Supplementary Fig. S2); and (2) there is a notable asymmetry between the occurrence of cold and hot days, particularly in mid- and high-latitude cities, with substantially more cold days prevailing. Our findings underscore the imperative for clarifying the dual impact of the UHI effect on annual net mortality across global cities, which holds particular importance for the broader scientific community and requires further clarification.

Note S7: ***Elucidation of assumptions in temperature-related mortality modeling***

Our present modelling strategies are based on static modelling assumptions, and do not distinguish between mortality due to indoor and outdoor temperature exposures. This approach is due to several factors and inherent limitations. First, regarding data and methodology, existing medical data provided by official agencies record daily total population deaths, which integrate both indoor and outdoor exposures[7,8], and do not differentiate between deaths resulting from indoor and outdoor exposures. This aggregation makes it challenging for previous attribution studies to separately evaluate temperature-related mortality due to indoor and outdoor temperatures. Thus, the methodological constraints of existing prediction models limit our ability to separately analyze mortality associated with indoor versus outdoor temperatures. Second, distinguishing deaths attributable to indoor versus outdoor exposures requires a detailed quantification of urban population dynamics. However, such quantification on a global scale is extremely challenging primarily because the dynamic attributes of urban population exposure are intricately influenced by factors such as urban population types, their mobility habits, and specific urban layouts[15]. Therefore, our approach, which employs a static assumption of continuous exposure for urban populations, aligns closely with prior large-scale exposure risk assessment studies[16-18]. Third, our primary aim is not to develop novel methods for more finely attributing temperature-related mortality, such as distinguishing between indoor and outdoor impacts. Instead, our main focus is on exploring the dual effects of UHI and urban cooling strategies on global temperature-related mortality, using established benchmarks. Therefore, employing a combined mortality-based assessment enhances comparability with existing research.

<u>Note S8:</u> ***Integration of the sWBGT index for assessing the impact of UHI on temperature-related mortality***

In this study, we consistently employed the air temperature index for assessing temperature-related mortality in global cities. This choice was made to maintain consistency with raw data from epidemiological studies and their accessibility. However, it is reasonable to consider that the wet bulb temperature index, which combines temperature and humidity, might provide a more accurate reflection of the risk of temperature-related mortality[19, 20]. To address this, we incorporated the simplified Wet Bulb Globe Temperature (sWBGT) index[21] into our assessment for comparative validation of our core findings.

We initially calculated the daily sWBGT index for global cities, utilizing both air temperature and humidity data[22]. We then established the sWBGT intensity at corresponding percentiles of the index for these cities. Applying a similar methodology, we estimated the dual impact of UHI effects on temperature-related mortality within an sWBGT index-based assessment framework. By juxtaposing these results with those from the air temperature index-based assessment, we assessed the sensitivity of our conclusions to the choice of assessment index.

Our results indicate a high correlation between the two assessments, with correlation coefficients of 0.88, 0.86, and 0.76 for heat-related mortality, cold-related mortality, and annual net mortality, respectively (Fig. S22a-c). Generally, UHI intensifies heat-related mortality while reducing cold-related mortality (Fig. S22a, b). Overall, the mitigating effect of UHI on cold-related mortality outweighs its intensifying effect on heat-related mortality, resulting in a net reduction in temperature-related mortality

(Fig. S22c).

We noted some variation in the impacts of sWBGT index-based and air temperature index-based UHIs on temperature-related mortality. For example, in the context of heat-related mortality, the sWBGT index-based UHI has a slightly more pronounced intensifying effect than its air temperature index-based counterpart (Fig. S22a). This suggests that incorporating humidity into the index amplifies the heat-related risk, leading to a more significant negative impact on heat-related mortality. This is further substantiated by regional results, where the sWBGT index-based UHI demonstrates a stronger intensifying effect on heat-related mortality in certain tropical cities (Fig. S22e).

Despite these variations, the sWBGT index-based and air temperature index-based assessments essentially reach the same conclusion on a global and multiple regional scales: the mitigating effects of UHI on cold-related mortality generally outweigh its intensifying effects on heat-related mortality, resulting in a net beneficial effect globally (Fig. S22 d-e; Fig. 2h, i). Notably, UHI significantly reduces cold-related mortality in cold and warm zones, as well as in cities across Europe and Oceania (Fig. S22d-e; Fig. 2h, i), indicating a clear net benefit. These results suggest that while there are minor variations in values from different indices, the key conclusions remain consistent and do not significantly alter the primary findings of our study.

The consistency across different indices largely stems from the fact that assessments using various moist heat indices consistently show that the adverse effects of temperature persist longer during cold periods[23]. This aligns with widespread findings based on air temperature, which often report a higher incidence of cold-related mortality. Such consistency reinforces our main findings regarding the dual impact of UHI on temperature-related mortality, emphasizing its protective role during cold periods over its adverse effects during heat.

Our choice to use air temperature for our assessments primarily derives from the fact that most available epidemiological studies use air temperature metrics to estimate temperature-related mortality. The aim of this study is to address the knowledge gap concerning the dual impacts of UHI on temperature-related mortality in cities worldwide. The use of air temperature, a standard metric in epidemiological research[7,8,24-26], allows for a direct comparison of our findings with most existing studies.

<u>Note S9:</u> ***Integration of meteorological station observations for assessing the impact of UHI on temperature-related mortality***

Given its broad coverage, we integrated the global air temperature estimate[27] into our calculation of UHI intensity for global cities. This data was subsequently used to comprehensively assess the dual impacts of UHI on temperature-related mortality on a global scale. However, considering the complexities of urban microclimates, one might question whether this air temperature estimate accurately captures the microclimate effects in urban areas, which could influence the assessment of UHI effects on temperature-related mortality. To address this, we supplemented our analysis with air temperature data from meteorological observation stations for comparative assessment, thereby testing the robustness of our findings.

Specifically, we obtained air temperature data from the global meteorological observing stations included in the Berkeley Earth dataset[28]. This dataset offers long time-series monthly near-surface air temperature data from over 40,000 meteorological stations worldwide and is widely used in urban climate research[29,30]. Initially, we filtered the air temperature data from urban and suburban stations provided by this dataset[31, 32], retaining those stations with data for all 12 months and eliminating outliers using a triple standard deviation method[33]. This process resulted in a selection of 2,076 urban stations and 5,512 suburban stations. Subsequently, we performed urban-suburban station matching[33-35], retaining only those cities with both types of stations. This matching process led to the inclusion of more than three hundred cities worldwide. We then quantified the monthly UHI intensity of these cities by calculating the mean air temperature difference between urban and suburban stations. Similar to our original approach, we used the UHI intensity—based on meteorological station data—to assess the additional impact of UHI on temperature-related mortality. Finally, we compared the UHI impact results derived from station data with those obtained from remotely sensed air temperatures to validate the robustness of our findings.

The results from over 300 cities consistently indicate that UHI's mitigating effect on cold-related mortality generally outweighs its exacerbating effect on heat-related mortality (Fig. S23a, b), suggesting an overall net beneficial impact of UHI on temperature-related mortality. Notably, in cities within cold, warm, and arid zones, UHI's mitigating effect on cold-related mortality significantly outweighs its exacerbating effect on heat-related mortality, leading to a clear net beneficial impact (Fig. S23c, d). Conversely, in some tropical cities, UHI's exacerbating effect on heat-related mortality is more pronounced, resulting in a net negative impact in parts of these cities (Fig. S23c, d). We also noted slight discrepancies in the UHI impact assessment in some Asian cities when comparing results based on station-based air temperatures and remotely sensed air temperatures. These discrepancies could be attributed to the small sample size of cities included, potentially introducing minor variations in assessments across different datasets. However, the conclusions derived from assessments in this region remain consistent across both datasets: UHI's mitigating effect on cold-related mortality in Asian cities generally outweighs its exacerbating effect on heat-related mortality (Fig. S23a, b).

In conclusion, despite minor numerical differences between the assessments based on the two datasets, the key conclusions are consistent: the average mitigating effect of UHI on cold-related mortality outweighs the average exacerbating effect on heat-related mortality across all assessed cities, indicating an average net positive impact. This finding aligns with the original overall conclusion of the study, further reinforcing the reliability of our results.

<u>Note S10:</u> ***Indicator considerations for the estimation models employed in this study***

This study involves three distinct random forest (RF) models: the temperature-mortality (M-T) association prediction model, the slope correction model for the effectiveness of cooling strategies, and the future UHI intensity prediction model. Each model utilizes different variables tailored to its specific objectives.

Prior studies indicate that the M-T relationship is influenced by a combination of climate (e.g., air temperature)[36], geographic factors (e.g., elevation, latitude)[37-39], economic conditions[40-42], and demographic profiles[43-45]. Based on these insights, we included ten categories of indicators – surface air temperature (SAT), dew point temperature, precipitation, wind speed, elevation, latitude/longitude, GDP, demographic structure (proportion of population over 65 years old), critical infrastructure spatial index (CISI), and human development index (HDI) as proxies for climatic and socio-economic factors in modeling M-T relationships.

The effectiveness of urban cooling strategies is linked to both the climatic conditions and urban development levels of a city. Previous analysis reveals that cooling strategy efficacy varies significantly across different climatic zones, with key climatic variables such as temperature and wind speed showing a notable inverse correlation with cooling effectiveness[46-48]. Additionally, urban development degree has been identified as a critical determinant influencing cooling strategy outcome[46]. To accurately model these dynamics, we selected a comprehensive set of indicators. From a climatic perspective, our model includes air temperature, dew point temperature, precipitation, and wind speed. To address the urban-specific factors, we considered urban population size, vegetation cover, albedo, and radiation levels.

Moreover, we incorporated geographical variables such as elevation and latitude/longitude to enhance the model's comprehensiveness and its ability to generalize across different urban settings.

In urban climate studies, UHI intensity is widely acknowledged to be closely associated with both the prevailing climatic conditions such as air temperature and precipitation and the extent of urbanization such as urban population size within a city[49,50]. These elements define the climatic and environmental disparities between urban and suburban areas, thereby influencing UHI intensity. Therefore, accurate prediction of UHI intensity across global cities necessitates the inclusion of these critical indicators. Given our focus on future predictions of UHI intensity, it is crucial to select indicators that will remain relevant and for which future data projections are available. In this regard, we have chosen indicators that best represent the climatic and urbanization factors likely to influence future UHI trends. These include air temperature, humidity, precipitation, urban population size, and geographic coordinates (latitude and longitude). This selection ensures that our model can effectively predict UHI intensity while accommodating variations in data availability and urban development scenarios globally.

Note S11: ***Analyses of vegetation and albedo in relation to temperature change in global cities***

The analysis of vegetation and albedo adjustment strategies in relation to temperature changes across global cities includes two stages: initial slope fitting and slope adjustment. In accordance with previous studies[51-53], we utilized the slopes of the linear regression relationship between temperature and vegetation/albedo to assess the impact of increasing vegetation and albedo strategies on temperatures across global cities. The absolute correlation coefficients (*r*) for the monthly relationship between vegetation changes and temperature are mainly in the range of 0.4 to 0.6 (Fig. S24a). The *r* values remain relatively consistent across months. For most cities, the significance levels (*p*) is less than 0.01 (Fig. S24b), suggesting a significance level exceeding 99%. The mean *r* values for the linear relationship between temperature and albedo remain stable around 0.42 (Fig. S24c), with a similarly high proportion of cities having *p*-values less than 0.01 (Fig. S24d). These results indicate that the linear relationships between cooling strategies (increasing vegetation and albedo) and temperature provides a stable and significant fitting performance for most cities worldwide.

The pixel-scale linear fittings could be affected by the limited samples and data quality issues, leading to anomalous (e.g., positive correlations due to outliers) values or insignificant fittings in a few cities. To ensure robust analysis, we first eliminated such outliers[54]. Based on the remaining results with outliers discarded, we then constructed correction models of the slopes by integrating various climate and urban characteristic variables (including air temperature, dew point temperature, precipitation, wind speed, urban population, vegetation cover, albedo intensity, radiation, elevation, and latitude/longitude information). By this approach, cities with missing fitting results can be well simulated using information from neighboring cities or cities with similar climatic conditions. Furthermore, the fitted slopes for cities can also be optimized and smoothed simultaneously after incorporating more information from adjacent cities. Note that the effectiveness of cooling strategies was evaluated separately during warm and cold months (identified using MMT estimates).

To validate the prediction model regarding the fitted slopes between vegetation/albedo and temperature, we conducted two categories of validation. First, we randomly divided the monthly fitted slope values of vegetation/albedo and temperature into two sets: 80% of the data for model training and the remaining 20% for model validation. Validation exhibits a correlation (r) of 0.77 and an R^2 of 0.57 for vegetation-temperature slopes, and a correlation (r) of 0.75 with an R^2 of 0.56 for albedo-temperature slopes (Fig. S25a, b). Despite a slight bias in a small part of the fitted slopes with high values, validation shows generally acceptable overall accuracies, with the vegetation-temperature slopes demonstrating a mean absolute error (MAE) of 0.60 °C. Second, the model generalizability was further corroborated through a tenfold randomization of the training and validation samples, yielding a consistent mean r and R^2 of 0.76 and 0.58 for vegetation, and 0.71 and 0.51 for albedo, respectively. The MAE values are 0.59 °C and 0.94 °C for vegetation and for albedo, respectively (Fig. S25c-f). These validations demonstrate acceptable generalization capabilities of the developed models.

Note S12: ***Possible uncertainties and limitations of this study***

There are several limitations in our study that point to promising directions for future research. For example, our representation of urban vegetation across global cities relied on the MODIS EVI products, which offers a broad global perspective but lacks the ability to accurately differentiate the vegetation types within cities. The current shortage of high-resolution data on vegetation type across global cities precludes our ability to delve into detailed vegetation analysis. We have proposed vegetation regulation strategies that entail minimal EVI growth intensities, thus reducing maintenance demands and preventing undue strain on urban systems. However, we acknowledge that the consideration of maintenance needs remains not fully addressed. As data availability expands, future studies should consider incorporating more meticulous vegetation data to improve accuracies by accounting for the unique cooling effects and maintenance needs of various vegetation types.

In addition, our model assumes static conditions and it does not account for the dynamic nature of urban populations, such as indoor-outdoor movements and location-specific exposure (Supplementary Note S7). Our proposed vegetation and albedo regulation scenarios (increases ranging from 4% to 40%) were designed under relatively ideal conditions, without considering practical constraints like city-specific building layouts, implementation feasibility, and potential interactions between urban vegetation and albedo changes. Furthermore, certain weather conditions such as snowfall can alter surface albedo and induce uncertainties in evaluating the impacts of albedo modifications on urban temperatures in some cities.

We have demonstrated that delicate machine learning extrapolation of the M-T association would not invalidate our core findings (Supplementary Note S3 to S6). However, practitioners should be cautious when employing machine learning-derived M-T associations in mortality studies that demand precise M-T curve data. It is also important to note that machine learning approaches cannot replace the traditional collection of M-T data from hospitals, especially in Global South cities where reliable data remains limited. Our M-T projection model, drawing from globally available data, integrates ten major categories of predictors. Nevertheless, we recognize that our estimation may not incorporate all relevant factors − for instance, urban migration characteristics are not adequately addressed. When assessing future temperature-related mortality, we, like previous studies[55], have applied relationships derived from historical data to future projections. This approach does not consider important factors such as human adaptation and urban development over time[56]. Our analysis implies that, within a moderate emission trajectory, the common cooling strategy is poised to yield more detriments than benefits regarding temperature-related mortality around 2050 for most mid-latitude cities (Supplementary Fig. S9). However, projections suggest that the increase in heat-related mortality instigated by the UHI effect should outweigh the decrease in cold-related mortality across cities in Central and Southern Europe and South America during the latter half this century[56]. It is important to note that our current estimates are grounded in temperature-mortality curves derived primarily from mortality data collected in the early years, around 2000[7]. This raises the concern that the mortality data from this period may no longer reflect current climatic conditions, particularly for cities that have witnessed an increase in extreme heat events, such as Phoenix and Los Angeles in the United States[57]. Furthermore, our estimates do not consider the substantial and abrupt surge in heat-related mortality arising from extreme heat events[58], which are expected to gain prominence under global warming scenarios[59]. In this changing climate landscape, the UHI effect in many mid-latitude cities might yield an annual net adverse impact even significantly before 2050 under low or moderate emission pathways. Furthermore, the data we used, from existing studies, are mostly based on daily-scale mortality assessments. As more detailed disease data become available in the future, investigating the hourly temperature-mortality relationship would be pivotal for improving our understanding of temperature impacts on urban mortality. Finally, we used city-wide spatial averages and monthly temporal averages to quantify the urban heat (or cool) island effect. Note that this effect is characterized by intra-city and intra-day variations. Future research should consider the more detailed spatiotemporal heterogeneity in this effect to enhance accuracy.

Despite these limitations, we consider the core finding remains robust – the mortality reduction induced by the UHI effect during cold spells can offset and even surpass the mortality increases during hotter periods. This finding holds because (1) cities worldwide are more frequently exposed to cold- than heat-related risks, and (2) the global mean MMP significantly exceeds 50% (Supplementary Fig. S2). We acknowledge that for a small subset of cities, primarily in tropical zones, the number of 'heat days' can outnumber 'cold days', leading to higher increases in heat-related mortality. However, the broader global urban population can obtain more benefits from the UHI effect and endure fewer detriments annually, resulting in a net global benefit (Supplementary Fig. S2a). This is also evidenced by the M-T relationships in individual cities such as Madrid and Tokyo, which demonstrate net positive health impacts induced by the UHI effect (Supplementary Fig. S2).

634

B. Supplementary Figures

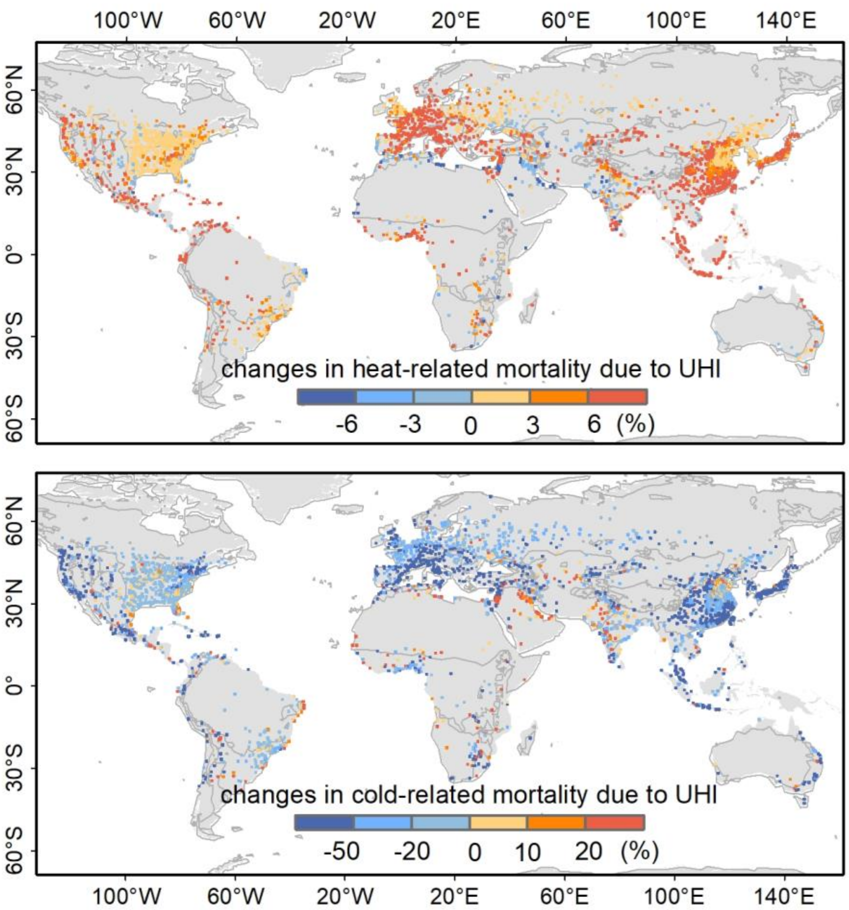

Fig. S1. Impact of the urban heat island (UHI) effect on heat-related mortality and cold-related mortality across global cities.

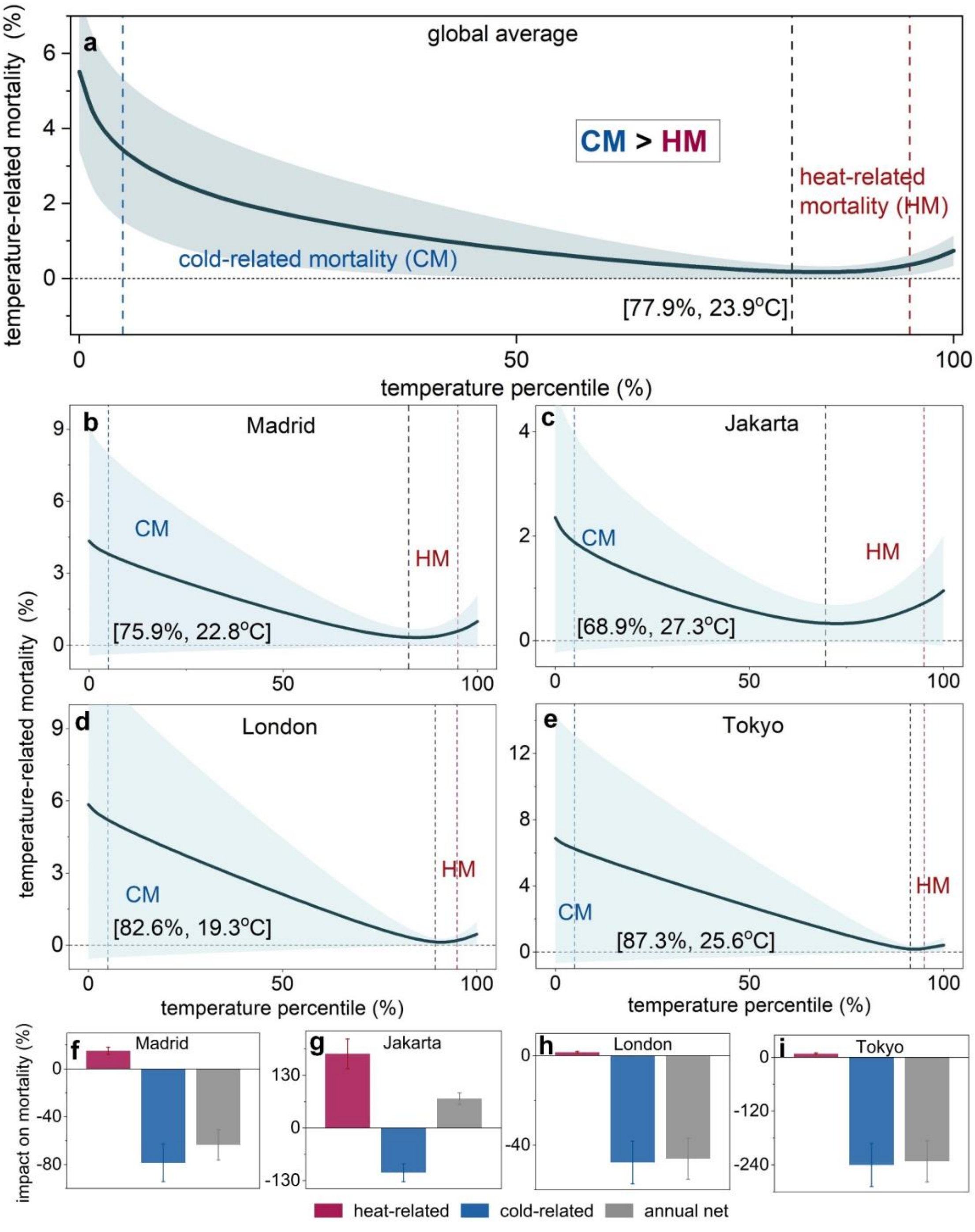

Fig. S2. The minimum mortality temperature (MMT, °C), minimum mortality percentile (MMP, %) and mortality changes (%) depending on temperature percentile | The results are for the global average (**a**) and several typical cities, including Madrid (**b**), Jakarta (**c**), London (**d**), and Tokyo (**e**); **f-i** show the UHI-induced mortality for heat-related (red boxplots), cold-related (blue), annual net conditions (grey) for Madrid (**f**), Jakarta (**g**), London (**h**), and Tokyo (**i**). The curves in Panel **a**-**e** indicate the variations in mortality related to temperature depending on temperature percentile. These have been fitted with a B-spline function for illustrative purposes, and the blue, grey, and red dashed lines indicate the 5% temperature percentiles, MMP, and 95% temperature percentiles, respectively. The shadow area in **a** to **e** denote one standard deviation of the variations in mortality related to temperature across all heat days and cold days. At the global scale, cold-related mortality (CM) is significantly greater than heat-related mortality (HM; CM > HM). This is true for Madrid, London, and Tokyo, while the CM is only marginally greater than the HM for Jakarta. The error bars in **f**-**i** denote one standard deviation of the impacts of UHI effects across all heat days, cold day, and full year (i.e., 365 days).

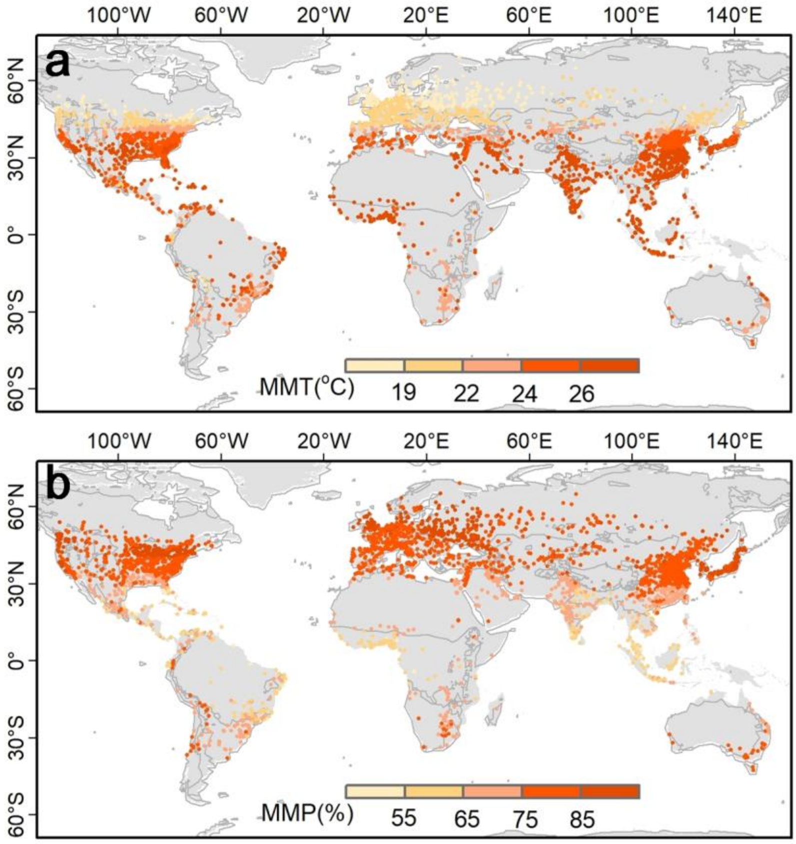

Fig. S3. The MMT and MMP estimates across global cities.

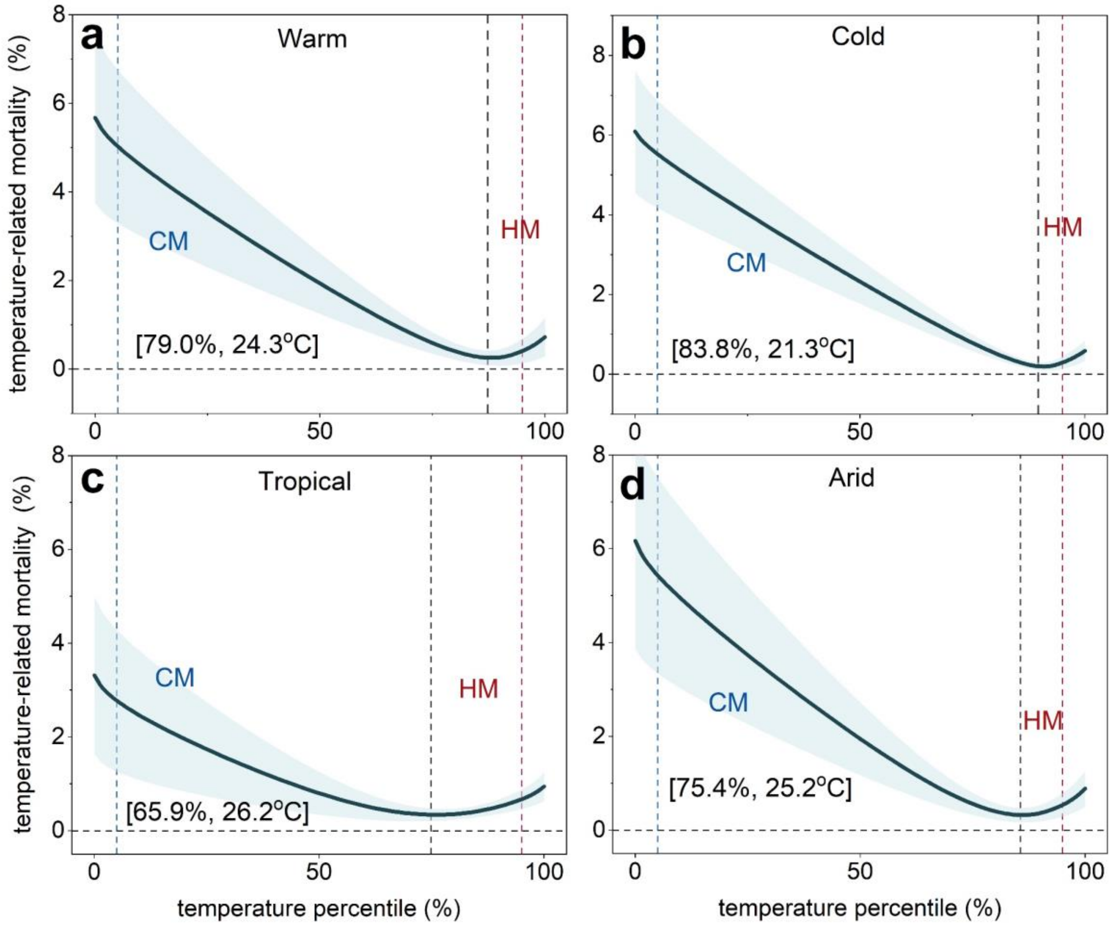

Fig. S4. The MMT (°C), MMP (%), and cumulative mortality changes (%) depending on the temperature percentile (%) for cities in various climate zones | The curves in Panel **a-d** indicate the variations in mortality related to temperature depending on temperature percentile. These have been fitted with a B-spline function for illustrative purposes. The shadow area denotes one standard deviation of the variations in mortality related to temperature across all heat days and cold days in regions. The blue, grey, and red dashed lines indicate the 5% temperature percentiles, MMP, and 95% temperature percentiles, respectively.

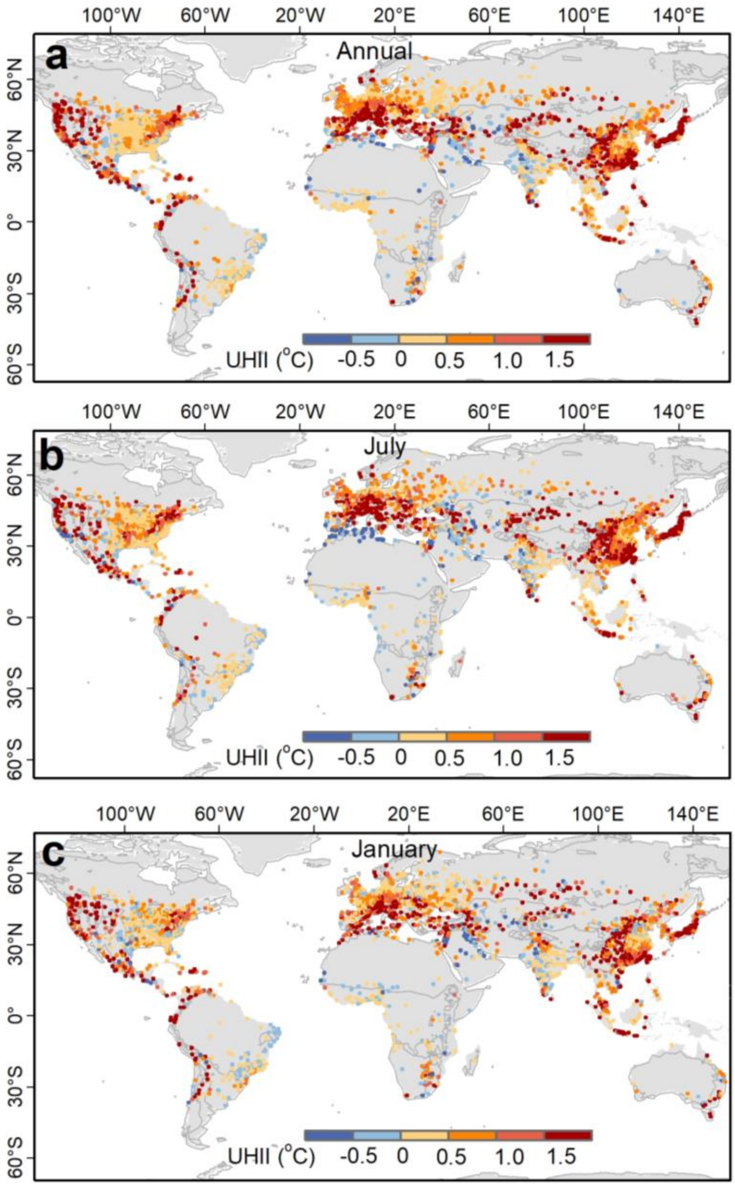

Fig. S5. Urban heat island intensity (UHII) across global cities in 2018 | **a** shows the annual mean UHII. **b** and **c** show the mean UHII in July and January, respectively.

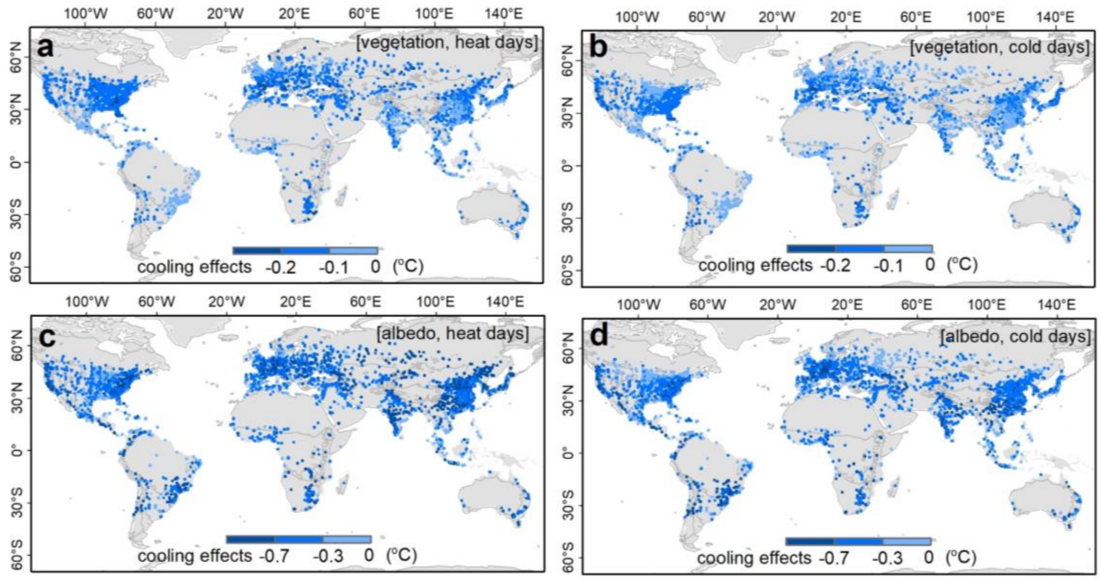

Fig. S6. Cooling effects of vegetation and albedo strategies across global cities | a and **b** denote the cooling effects of increasing vegetation by 40%, 30%, and 20% for cities with low, medium, and high population density, respectively, in heat days and cold days; **c** and **d** denote the cooling effects of increasing albedo by 40%, 30%, and 20% for cities with low, medium, and high albedo intensity, respectively, in heat days and cold days. The cooling effects were quantified by the reduction in urban surface air temperature.

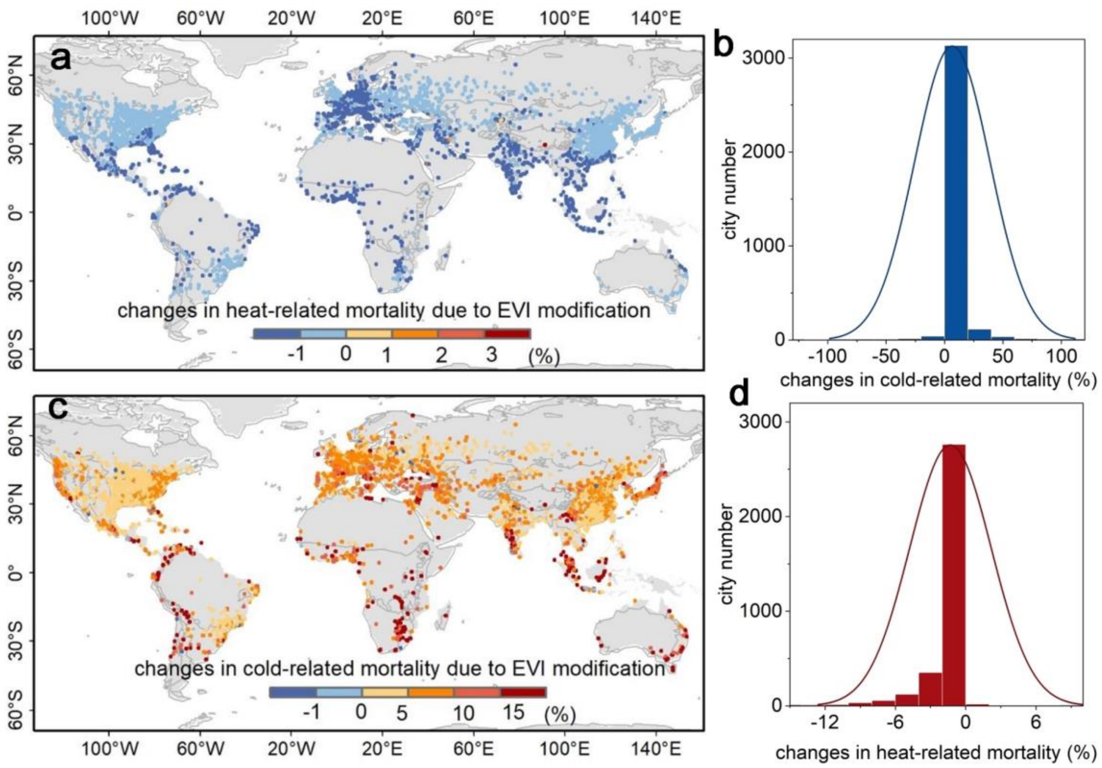

Fig. S7. Impacts of vegetation increase strategy on heat-related mortality and cold-related mortality across global cities | The specific strategy entails increasing vegetation by 40%, 30%, and 20% of the original cover for low, medium, and high population density cities, respectively.

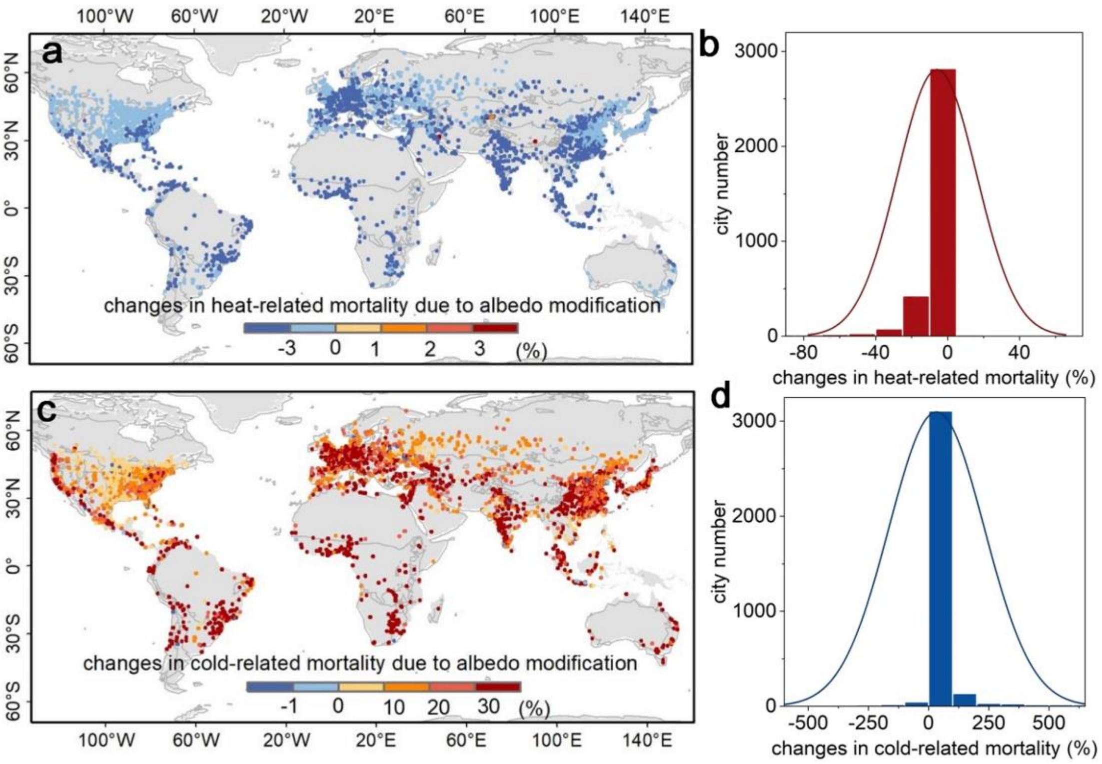

Fig. S8. Impacts of albedo increase strategy on heat-related mortality and cold-related mortality across global cities | The specific strategy entails increasing albedo by 40%, 30%, and 20% for low, medium, and high albedo intensity cities, respectively.

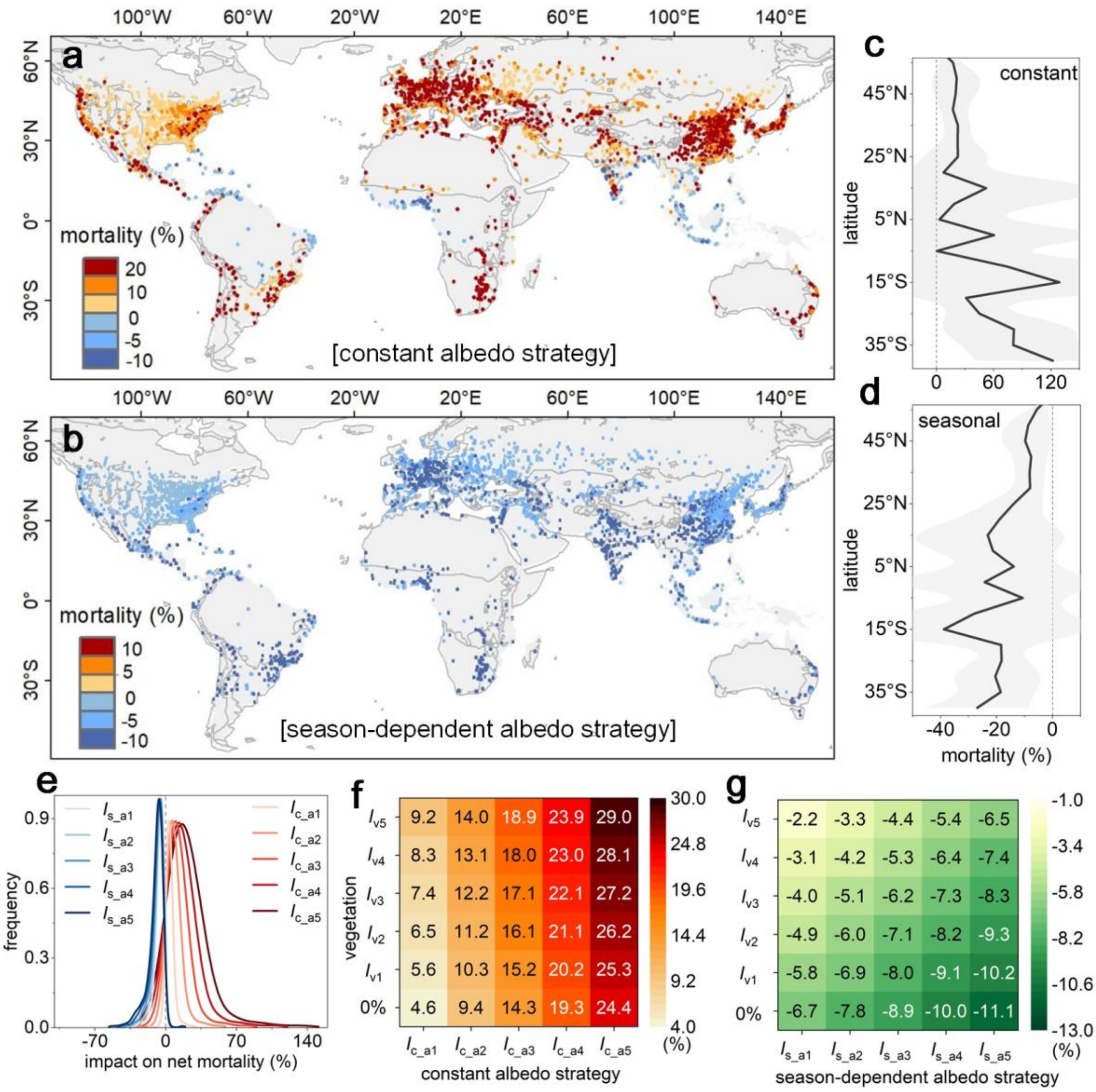

Fig. S9. Impacts of urban cooling strategies on cold- and heat-related mortality in 2050 under SSP2-4.5 | Impacts of two urban cooling strategies (by changing surface albedo) on the annual net mortality in global cities, i.e., the constant albedo strategy (i.e., increasing surface albedo in all year round; **a**) and the season-dependent albedo strategy (i.e., increasing surface albedo in warm season, while decreasing it in cold season; **b**); variations in future annual net mortality depending on latitude by implementing the constant (**c**) and season-dependent (**d**) albedo strategies; comparison of changes in annual net mortality using the constant and season-dependent albedo strategies with different regulation intensities (**e**); changes in annual net mortality by combining the implementation of increasing vegetation fraction and surface albedo (constant albedo strategy) with different regulation intensities (**f**); and **g** mirrors **f**, but for the season-dependent albedo strategy. The shadow area in **c** and **d** denote one standard deviation of the impacts of urban cooling strategies on each latitude range. 'I_{v1}' to 'I_{v5}' represent the vegetation regulatory intensity, with levels ranging from low (e.g., increases of 4%, 6%, and 8%) to high (e.g., increases of 20%, 30%, and 40%). '$I_{\mathrm{c\text{-}a1}}$' to '$I_{\mathrm{c\text{-}a5}}$' indicate the regulatory intensity of the constant surface albedo strategy, ranging from low (e.g., increases of 4%, 6%, and 8%) to high (e.g., increases of 20%, 30%, and 40%) levels. '$I_{\mathrm{s\text{-}a1}}$' to '$I_{\mathrm{s\text{-}a5}}$' denote the regulatory intensity of the season-dependent albedo strategy from low to high levels, i.e., surface albedo was increased at varying intensities during warm seasons, whereas it was decreased by 4%, 6%, and 8% of the initial condition for cities with high, medium, and low albedo intensity classes during cold seasons (see Methods). Positive values indicate a net increase in mortality due to a cooling strategy, and negative values indicate a decrease.

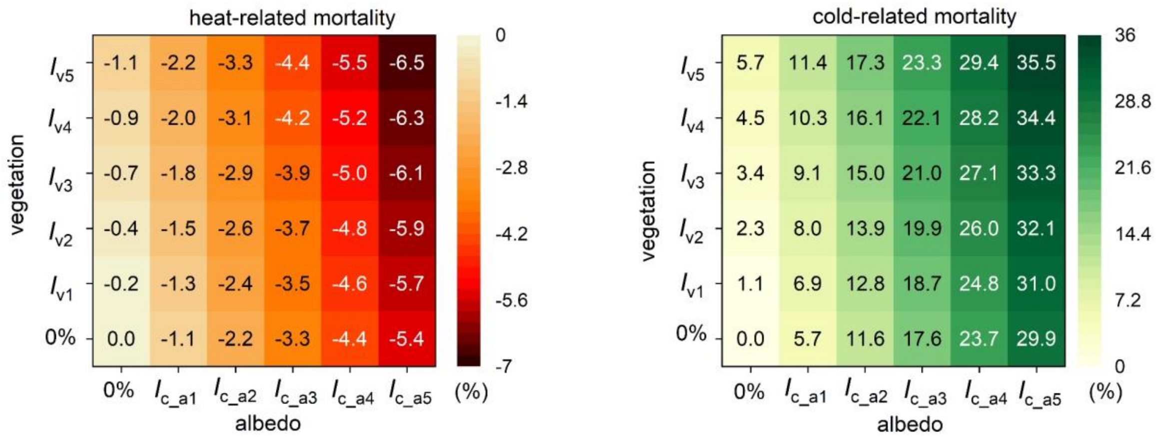

Fig. S10. Impacts of urban vegetation and albedo strategies on heat-related mortality and cold-related mortality in 2050 | The x-axis denotes the regulation intensity of albedo strategy, and the y-axis denotes the regulation intensity of vegetation strategy. 'I_{v1}' to 'I_{v5}' represent the regulatory intensity of the vegetation strategy, with levels ranging from low (e.g., increases of 4%, 6%, and 8%) to high (e.g., increases of 20%, 30%, and 40%). '$I_{c\text{-}a1}$' to '$I_{c\text{-}a5}$' indicate the regulatory intensity of the constant surface albedo strategy, ranging from low (e.g., increases of 4%, 6%, and 8%) to high levels (e.g., increases of 20%, 30%, and 40%; refer to Methods).

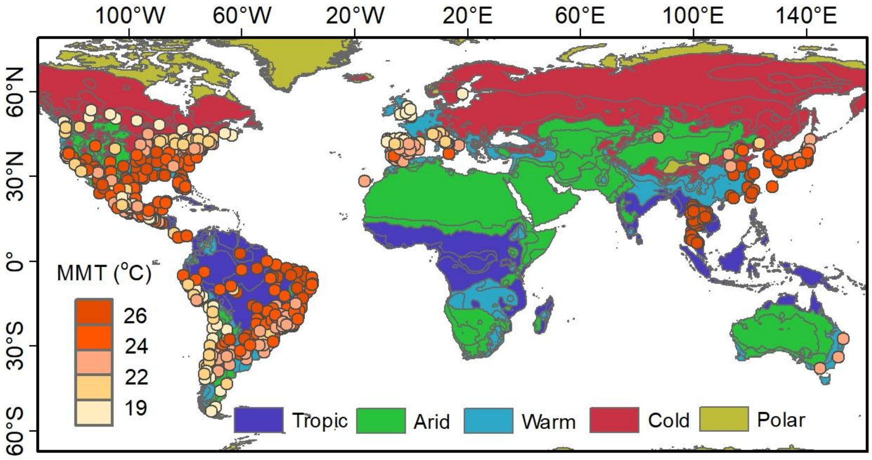

Fig. S11. Global distribution of sample cities with detailed mortality-temperature (M-T) associations across Koppen-Geiger climate zones | MMT (ºC) denotes the minimum mortality temperature.

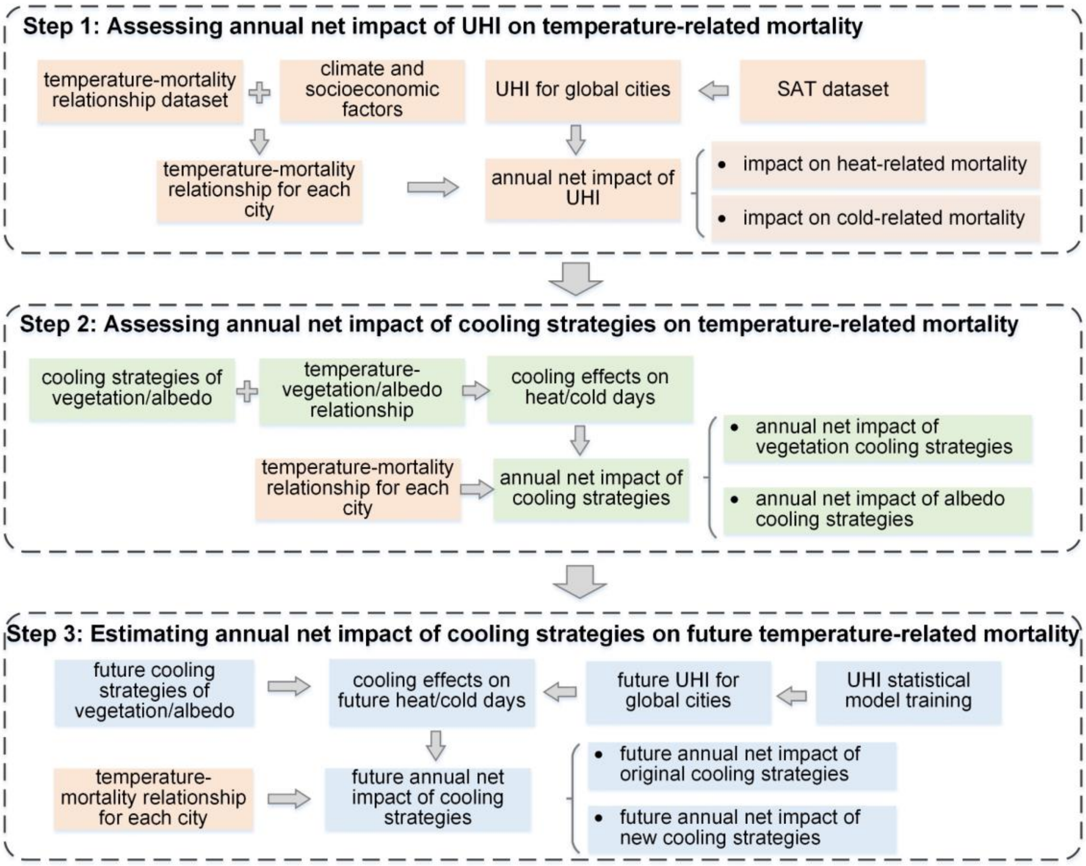

Fig. S12. A complete flowchart used for assessing the impacts of the UHI effect and cooling strategies on temperature-related mortality | UHI and SAT refer to urban heat island and surface air temperature, respectively.

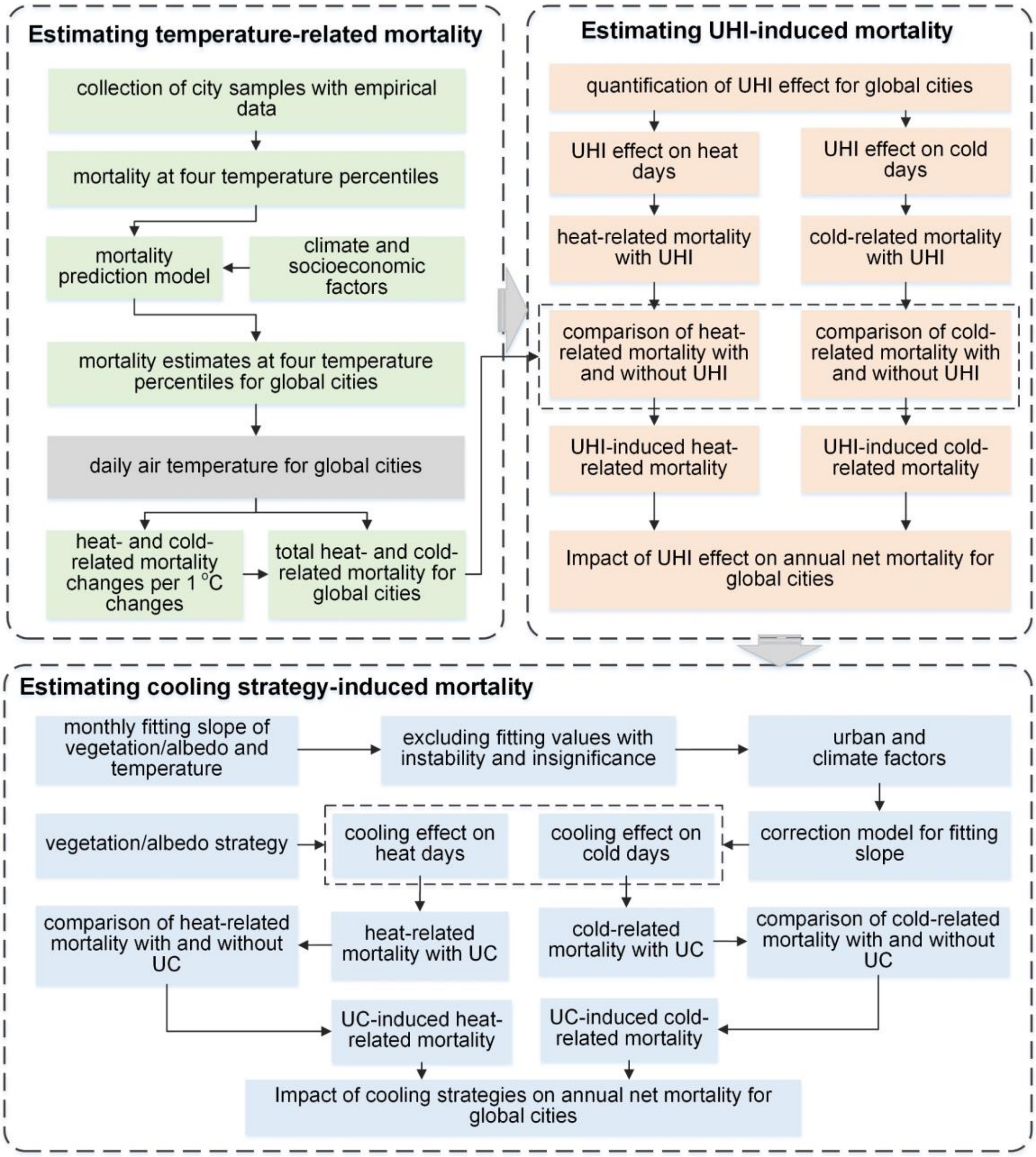

Fig. S13. Flowchart for quantifying the impact of the UHI effect and the associated cooling strategies on temperature-related mortality.

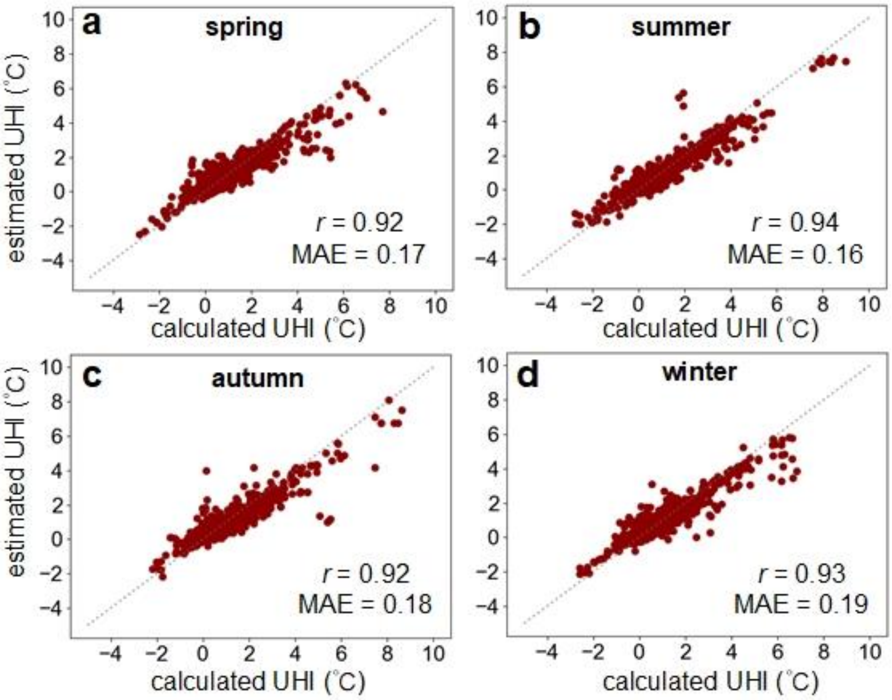

Fig. S14. Comparison between the original UHI intensity calculated by urban air temperature data and the UHI intensity estimated by a random forest model across global cities (with an urban area > 30 km^2 in 2010) for the four seasons from 2010-2014.

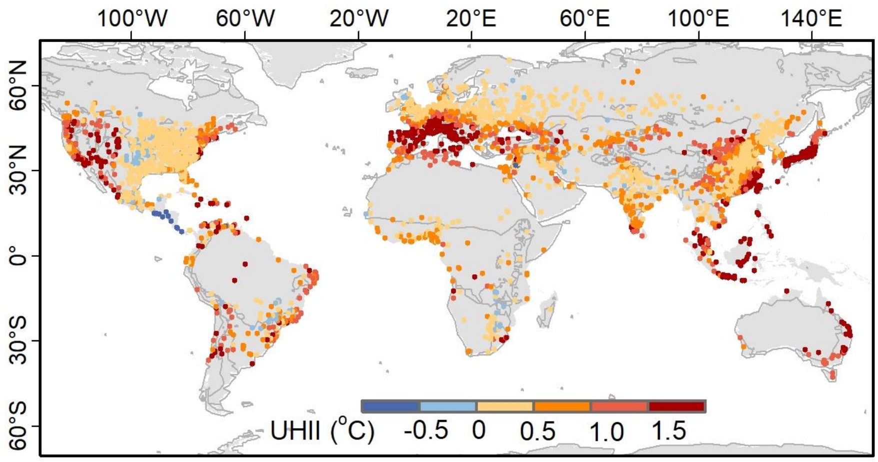

Fig. S15. Estimated annual mean UHII across global cities in 2050.

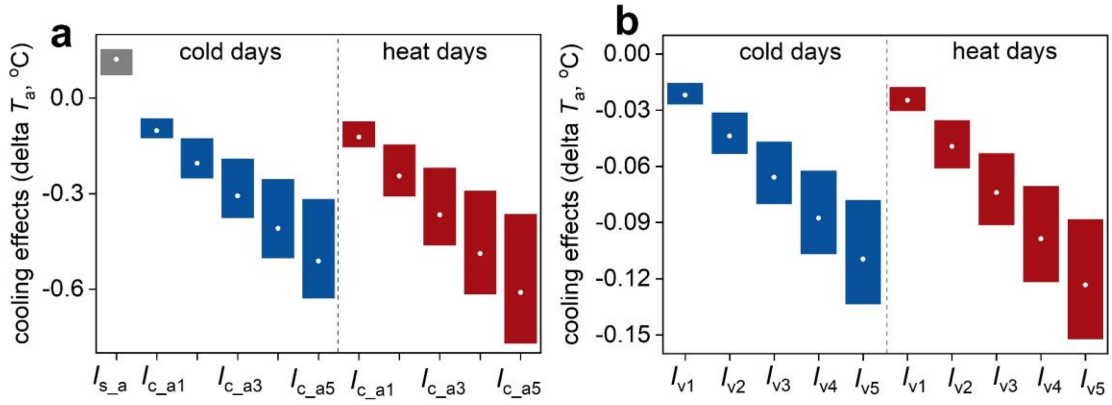

Fig. S16. Cooling effects of different albedo and vegetation strategies on cold and heat days | In subfigure (**a**), the 'red' and 'blue' bars denote the urban surface air temperature (SAT) reduction (delta T_a) when surface albedo is increased on heat and cold days, respectively, while the 'gray' bar demonstrates the urban SAT growth when surface albedo is decreased on cold days. In subfigure (**b**), the 'red' and 'blue' bars denote the urban SAT reduction when vegetation cover is increased on heat and cold days, respectively. 'I_{v1}' to 'I_{v5}' represent the regulatory intensity of the vegetation strategy, with levels ranging from low (e.g., increases of 4%, 6%, and 8%) to high (e.g., increases of 20%, 30%, and 40%). '$I_{c\text{-}a1}$' to '$I_{c\text{-}a5}$' indicate the regulatory intensity of the constant surface albedo strategy, ranging from low (e.g., increases of 4%, 6%, and 8%) to high (e.g., increases of 20%, 30%, and 40%). '$I_{s\text{-}a}$' denotes the regulatory intensity of the season-dependent albedo strategy, i.e., surface albedo was decreased by 4%, 6%, and 8% of the initial condition for cities with high, medium, and low albedo intensity classes on cold days.

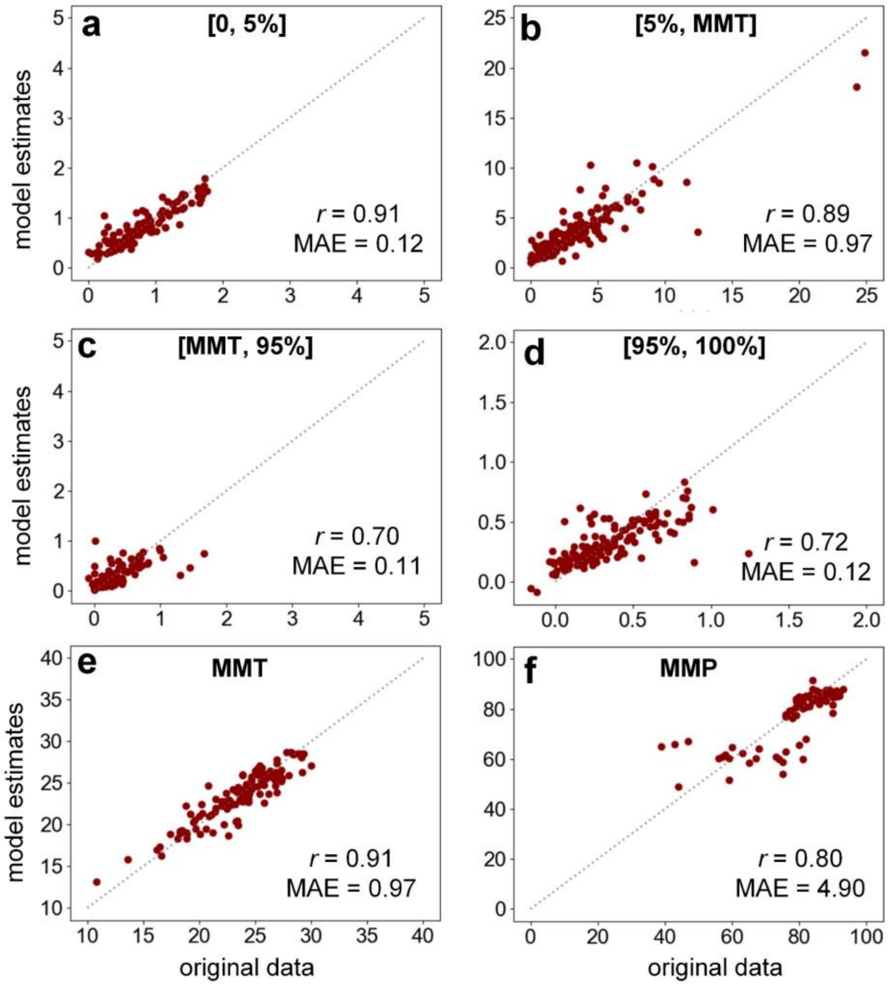

Fig. S17. Comparison between the original and estimated MMT (unit: ^{o}C; e), MMP (unit: %; f), and the cumulative mortality (unit: %) at temperature percentiles (i.e., 0 – 5%, 5% – MMT, MMT – 95%, 95 – 100%; a to d) using 80% of the data for training and 20% for validation.

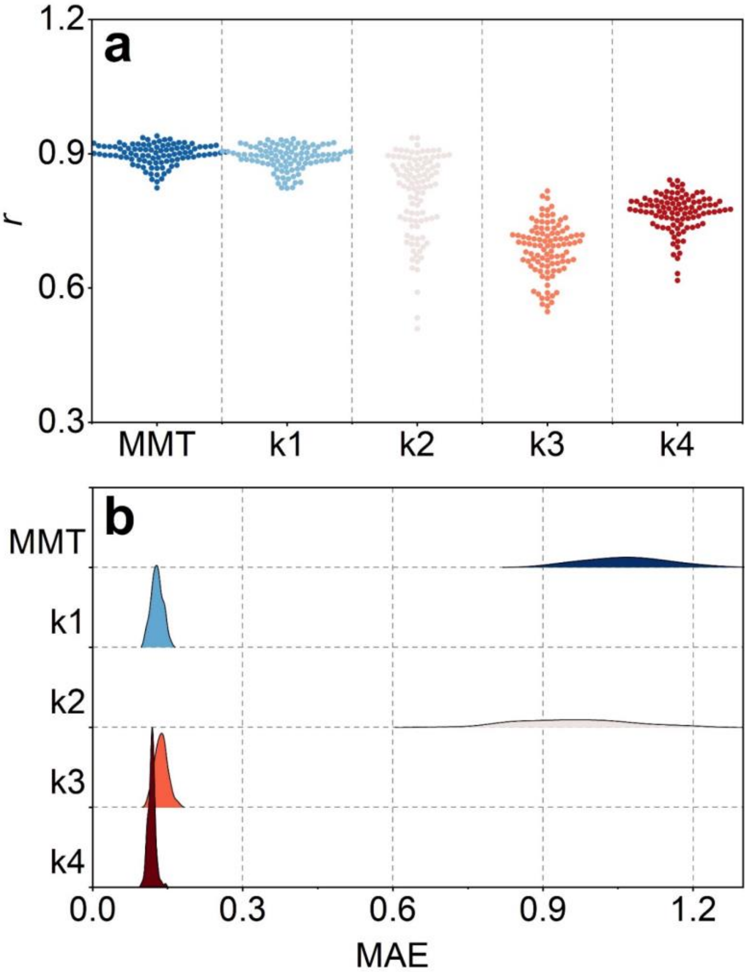

Fig. S18. Correlation coefficient (r) and mean absolute error (MAE) changes for the estimated MMT (unit: °C) and for the estimated cumulative mortality (unit: %) at different temperature percentiles for the 100 random splits when training the random forest model | The 'k1' to 'k4' represent the temperature percentile intervals of 0 – 5, 5 – MMT, MMT – 95, and 95 – 100, respectively.

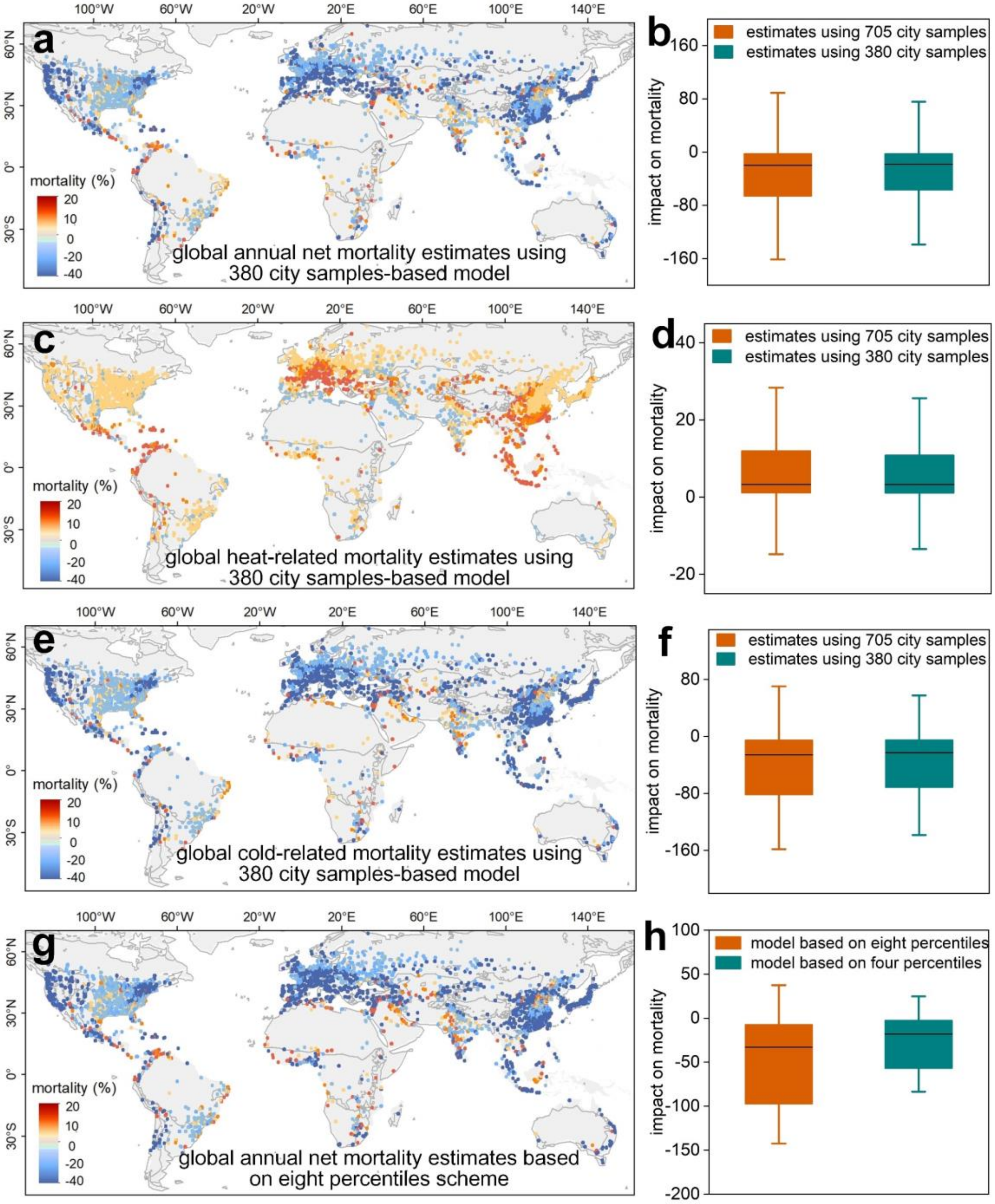

Fig. S19. Comparison of the UHI-induced temperature-related mortality across global cities using different city samples and scheme for modeling | a, **c**, and **e** show the UHI-induced annual, heat-related, and cold-related mortality for global cities estimated by combining the temperature-association data obtained from 380 city samples, respectively; **b**, **d**, and **f** show the comparison of UHI-induced annual, heat-related, and cold-related mortality estimates by combining the temperature-association data obtained from 705 city samples and from 380 city samples, respectively; **g** show the show the UHI-induced annual net mortality for global cities estimated by combining the temperature-association data obtained from 380 city samples using an eight percentiles division scheme (i.e., 0% – 2.5%, 2.5% – 10%, 10% – 25%, 25% – 50%, 50% – 75%, 75% – 90%, 90% – 97.5%, and 97.5% – 100%); and **h** shows the comparison of the UHI-induced annual net mortality by four-division (i.e., >5%, 5% – MMT, MMT – 95%, and >95%) and eight-division temperature percentile scheme, both based on the temperature-association data obtained from 380 city samples. In subplots **b**, **d**, **f**, and **h**, the solid line represents the median value, while the lower and upper lines denote 25th and 75th quantiles, respectively. The lower and upper bounds of the whiskers indicate the outlier range with an outlier coefficient of 1.

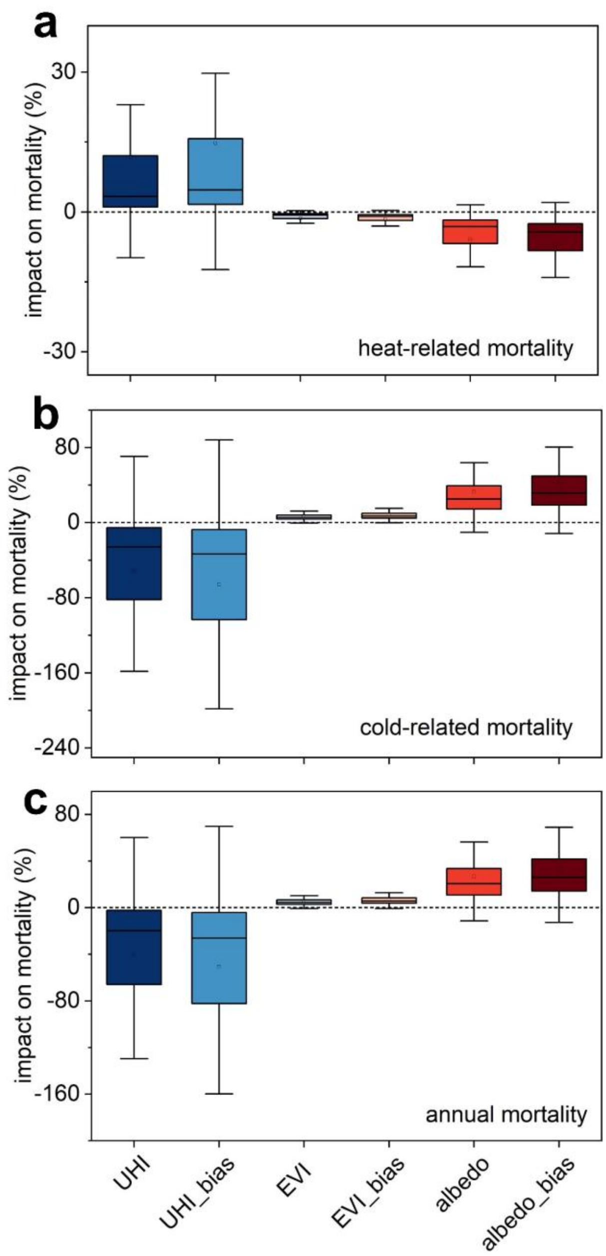

Fig. S20. Potential impacts of model biases on the heat-related, cold-related, and annual mortality estimates for global 3,280 cities | The 'UHI', 'EVI', and 'Albedo' along the x-axis denote the original estimated cumulative mortality due to the UHI effect, vegetation modification strategy, and albedo modification strategy, respectively. In contrast, 'UHI_bias', 'EVI_bias', and 'Albedo_bias' denote the estimated cumulative mortality due to the UHI effect and the vegetation and albedo modification strategies by considering model biases. In subplots **a** to **c**, the small box represents the mean value, and the solid line represents the median value; the lower and upper lines denote 25th and 75th quantiles, respectively, while the lower and upper bounds of the whiskers indicate the outlier range with an outlier coefficient of 1.5.

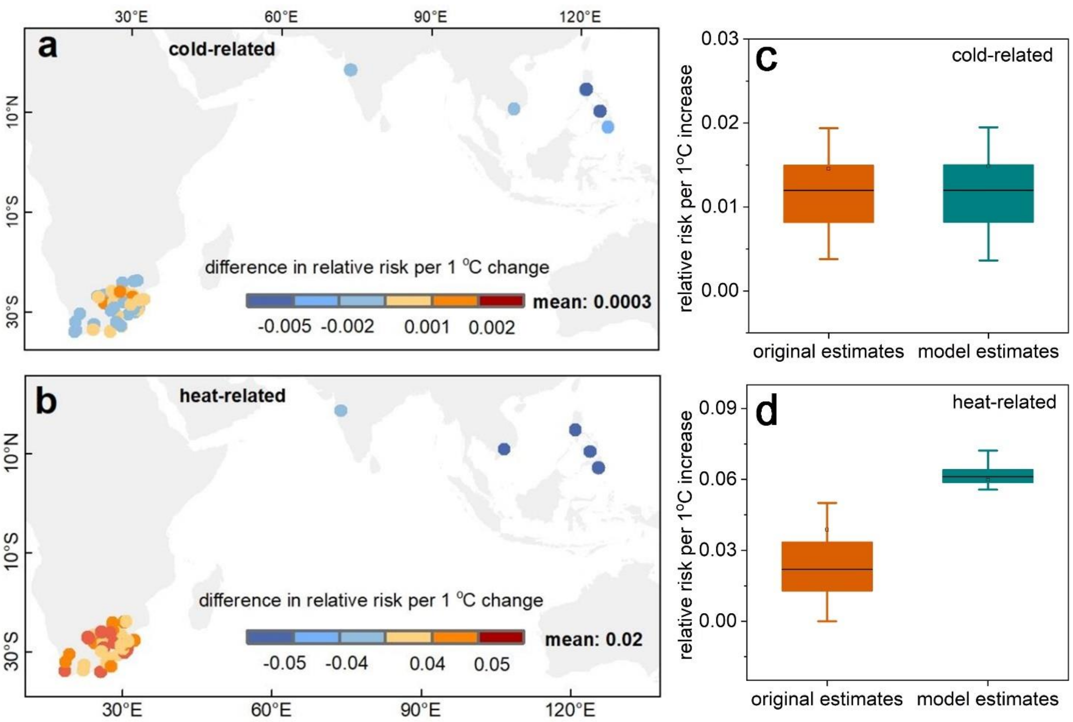

Fig. S21. Comparison of cold-related and heat-related mortality risk between the estimates derived from the prediction model and the original statistical results for 49 sample cities in Africa and South Asia | In subplots **c** and **d**, the small box represents the mean value, and the solid line represents the median value; the lower and upper lines denote 25th and 75th quantiles, respectively, while the lower and upper bounds of the whiskers indicate the outlier range with an outlier coefficient of 1.5.

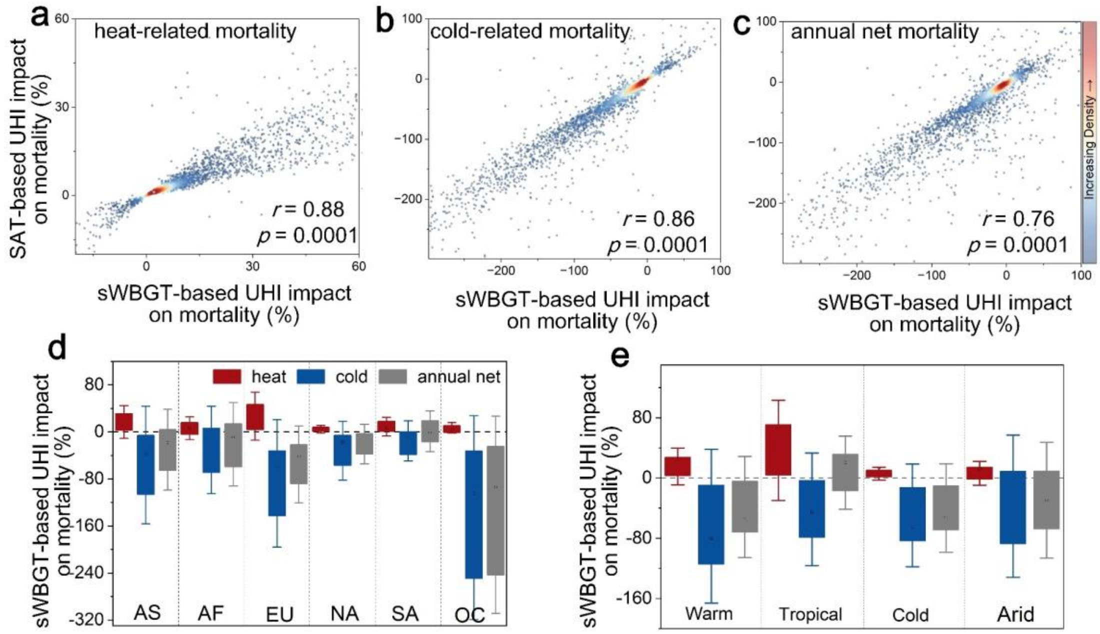

Fig. S22. Assessment of the UHI impact on temperature-related mortality globally based on the sWBGT index | a-c illustrate the sWBGT-based and air temperature-based UHI impacts on heat-related (**a**), cold-related (**b**), and annual net mortality (**c**), where the values refer to the cumulative impacts of the UHI on the temperature-related mortality from the daily scale for each city. **d-e** depict the continental (**d**; 1394 Asian cities, 196 African cities, 614 European cities, 841 North American cities, 188 South American cities, and 47 Oceanian cities) and climate zone (**e**; 1706 warm cities, 441 tropical cities, 754 cold cities, and 379 arid cities) statistics of the sWBGT-based UHI impacts on temperature-related mortality. AS: Asia, AF: Africa, EU: Europe, NA: North America, SA: South America, OC: Oceania. In subplots **d** and **e**, the small box represents the median value, while the lower and upper lines denote 25th and 75th quantiles, respectively. The lower and upper bounds of the whiskers indicate the outlier range with an outlier coefficient of 0.5. The *r* and *p* values in subplots **a** to **c** are derived from a two-sided *t*-test with no adjustments.

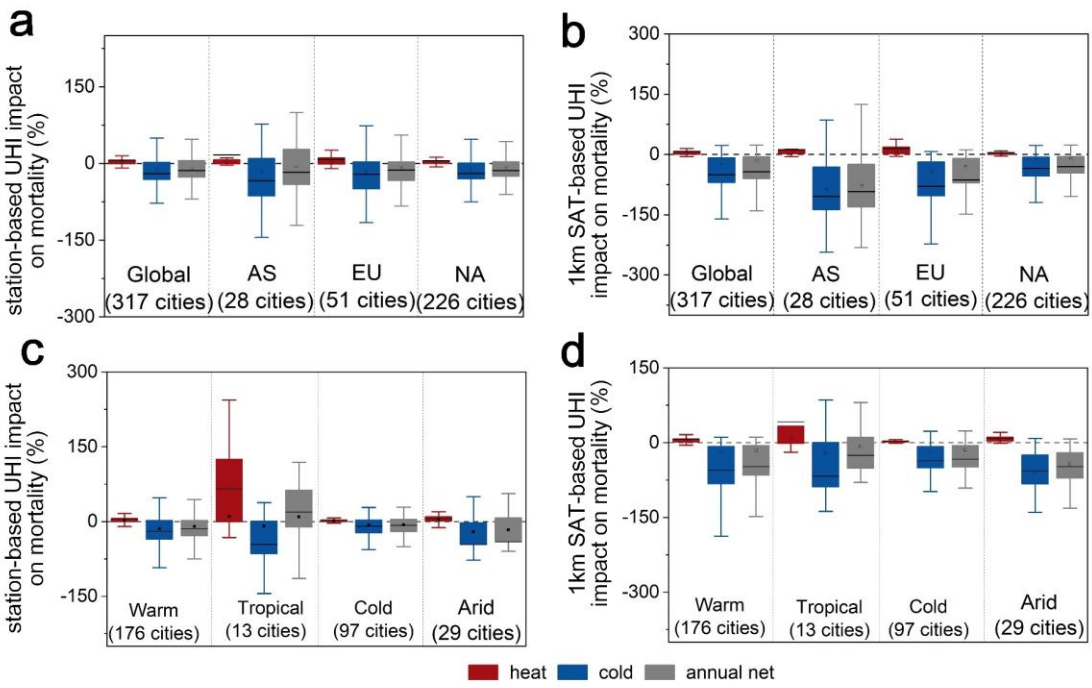

Fig. S23. Assessment of the dual effects of UHI on temperature-related mortality in 317 cities worldwide based on both meteorological station-based air temperatures and remotely sensed air temperatures | a-b show the results at global 317 cities and continental (28 Asian cities, 51 European cities, and 226 North American cities) scales, while **c-d** show the results at climate zone (176 warm cities, 13 tropical cities, 97 cold cities, and 29 arid cities) scales. Note that only continents and climate zones with more than 10 cities are shown, with the data in parentheses representing the number of cities. AS: Asia, EU: Europe, NA: North America. In subplots **a** to **d**, the solid line represents the mean value, and the small box represents the median value; the lower and upper lines denote 25th and 75th quantiles, respectively, while the lower and upper bounds of the whiskers indicate the outlier range with an outlier coefficient of 1.5.

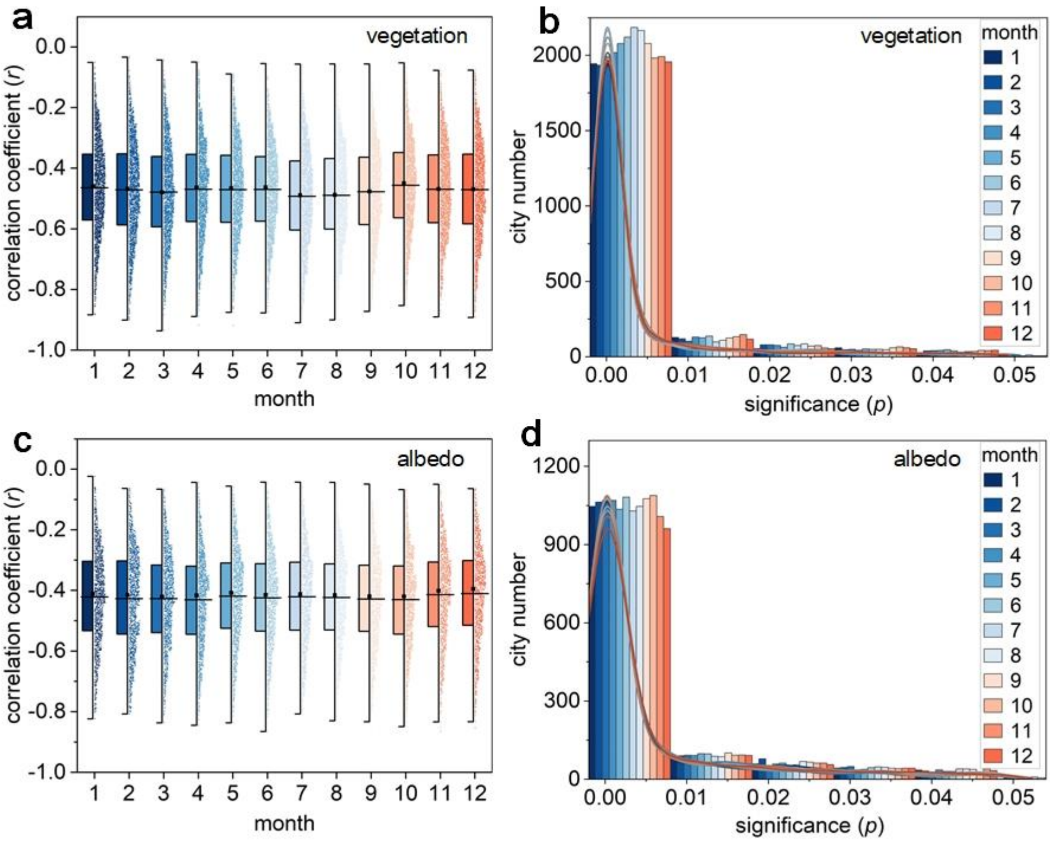

Fig. S24. The correlation coefficients (r) and significance levels (p) for the monthly linear relationship between the cooling strategies and air temperature in cities | In subplots **a** and **c**, the number of city samples from January to December are 2218, 2219, 2298, 2314, 2377, 2440, 2441, 2448, 2368, 2298, 2298, and 2225, respectively. The solid lines in **a** and **c** represent the mean values, while the dots represent the median values; the lower and upper lines denote 25th and 75th quantiles, respectively, while the lower and upper bounds of the whiskers indicate the outlier range with an outlier coefficient of 1.5. The *p* values in subplots **b** and **d** are derived from a two-sided t-test with no adjustments.

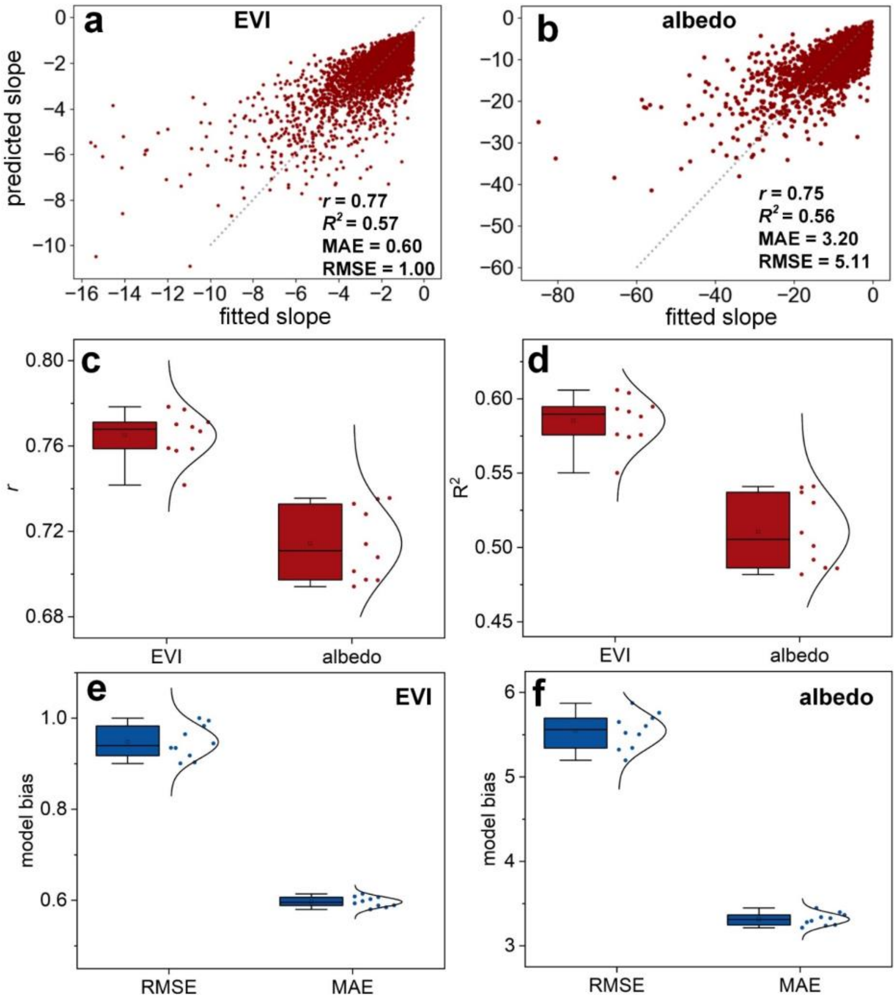

Fig. S25. Accuracy assessments on the fitted slopes between temperature and vegetation (albedo) | The numbers in subplots **c** to **f** represent ten result values through a tenfold randomization of the training and validation samples. The solid lines in **c** to **f** represent the median values, while the dots represent the mean values; the lower and upper lines denote 25th and 75th quantiles, respectively, while the lower and upper bounds of the whiskers indicate the outlier range with an outlier coefficient of 1.5.

C. Supplementary References

1. Krayenhoff, E. S. et al. Cooling hot cities: a systematic and critical review of the numerical modelling literature. *Environ. Res. Lett.* **16**, 053007 (2021).
2. Yang, J. & Bou-Zeid, E. Should cities embrace their heat islands as shields from extreme cold? *J. Appl. Meteorol. Climatol*. **57**, 1309–1320 (2018).
3. Santamouris, M. Using cool pavements as a mitigation strategy to fight urban heat island—A review of the actual developments. *Renew. Sust. Energ. Rev.* **26**, 224–240 (2013).
4. Rosso, F. et al. New cool concrete for building envelopes and urban paving: Optics-energy and thermal assessment in dynamic conditions. *Energ. Buildings* **151**, 381–392 (2017).
5. Ramamurthy, P. et al. Influence of subfacet heterogeneity and material properties on the urban surface energy budget. *J. Appl. Meteorol. Clim.* **53**, 2114–2129 (2014).
6. Xu, Q. S. & Liang, Y. Z. Monte Carlo cross validation. *Chemometr. Intell. Lab.* **56**, 1–11 (2001).
7. Gasparrini, A. et al. Mortality risk attributable to high and low ambient temperature: a multicountry observational study. *The Lancet* **386**, 369–375 (2015).
8. Kephart, J. L. et al. City-level impact of extreme temperatures and mortality in Latin America. *Nat. Med.* **28**, 1700–1705 (2022).
9. Scovronick, N. et al. The association between ambient temperature and mortality in South Africa: A time-series analysis. *Environmental research* **161**, 229-235 (2018).
10. Lee, W. H. et al. An investigation on attributes of ambient temperature and diurnal temperature range on mortality in five east-Asian countries. *Scientific Reports* **7**,

10207 (2017).

11. Ingole, V., Sheridan, S. C., Juvekar, S., Achebak, H. & Moraga, P. Mortality risk attributable to high and low ambient temperature in Pune city, India: A time series analysis from 2004 to 2012. *Environmental Research*, **204**, 112304 (2022).

12. Zhao, Q. et al. Global, regional, and national burden of mortality associated with non-optimal ambient temperatures from 2000 to 2019: a three-stage modelling study. *Lancet Planet. Health* **5**, e415–e425 (2021).

13. Gasparrini, A. et al. Projections of temperature-related excess mortality under climate change scenarios. *Lancet Planet. Health* **1**, e360-e367 (2017).

14. Martínez-Solanas, È. et al. Projections of temperature-attributable mortality in Europe: a time series analysis of 147 contiguous regions in 16 countries. *Lancet Planet. Health* **5**, e446–e454 (2021).

15. Babkin, R., Badina, S. & Mikhaylov, A. Intraday Dynamics of the Urban Population in Studies of Natural and Man-Made Risks (Case Study of Moscow, Russia). *In International Perm Forum Science and Global Challenges of the 21st Century* (2022).

16. Zhu, D., Zhou, Q., Liu, M. & Bi, J. Non-optimum temperature-related mortality burden in China: Addressing the dual influences of climate change and urban heat islands. *Sci. Total Environ*. **782**, 146760 (2021).

17. Jones, B. et al. Future population exposure to US heat extremes. *Nat. Clim. Change* **5**, 652-655 (2015).

18. Iungman, T. et al. Cooling cities through urban green infrastructure: a health impact assessment of European cities. *The Lancet* **401**, 577–589 (2023).

19. Mora, B. et al. Global risk of deadly heat. *Nat. Clim. Change* **7**, 501–506 (2017).

20. Raymond, C., Matthews, T. & Horton, R. M. The emergence of heat and humidity too severe for human tolerance. *Sci. Adv*. **6**, eaaw1838 (2020).

21. Buzan, J. R., Oleson, K. & Huber, M. Implementation and comparison of a suite of heat stress metrics within the Community Land Model version 4.5. *Geosci. Model Dev*. **8**, 151-170 (2015).

22. Muñoz-Sabater, J. et al. ERA5-Land: a state-of-the-art global reanalysis dataset for land applications. *Earth Syst. Sci. Data* **13**, 4349–83 (2021).

23. Rodopoulou S, et al. Searching for the best modeling specification for assessing the effects of temperature and humidity on health: a time series analysis in three European cities. *Int. J. Biometeorol.* **59**, 1585–1596 (2015).

24. Huang, Z. et al. Individual-level and community-level effect modifiers of the temperature-mortality relationship in 66 Chinese communities. *BMJ Open* **5**, e009172 (2015).

25. Wang, C. et al. Nonlinear relationship between extreme temperature and mortality in different temperature zones: a systematic study of 122 communities across the mainland of China. *Sci. Total Environ*. **586**, 96-106 (2017).

26. Guo, Y. et al. Heat wave and mortality: a multicountry, multicommunity study. *Environ. Health Perspect* **125**, 087006 (2017).

27. Zhang, T. et al. A global dataset of daily near-surface air temperature at 1-km resolution (2003–2020). *Earth Syst. Sci. Data Discuss*. **2022**, 1–18 (2022).

28. Rohde, R.et al. Berkeley Earth temperature averaging process. *Geoinformatics Geostatistics An Overview* **1**, 20-100 (2013).

29. Zhou, C. & Wang, K. Coldest temperature extreme monotonically increased and hottest extreme oscillated over Northern Hemisphere land during last 114 years. *Sci. Rep*. **6**, 25721 (2016).

30. Curci, G. et al. Building a local climate reference dataset: Application to the Abruzzo region (Central Italy), 1930–2019. *Int. J. Climatol*. **41**, 4414-4436 (2021).

31. Li, X. et al. Mapping global urban boundaries from the global artificial impervious area (GAIA) data. *Environ. Res. Lett*. **15**, 094044 (2020).

32. Yao, R. et al. Greening in rural areas increases the surface urban heat island intensity. *Geophys. Res. Lett*. **46**, 2204-2212 (2019).

33. Du, H. et al. Simultaneous investigation of surface and canopy urban heat islands over global cities. *ISPRS J. Photogramm*. **181**, 67-83 (2021).

34. Wang, W. C., Zeng, Z. & Karl, T. R. Urban heat islands in China. *Geophys. Res. Lett*. **17**, 2377-2380 (1990).

35. Tam, B. Y., Gough, W. A. & Mohsin, T. The impact of urbanization and the urban heat island effect on day to day temperature variation. *Urban Clim*. **12**, 1-10 (2015).

36. Krummenauer, L. et al. Global drivers of minimum mortality temperatures in cities. *Sci. Total Environ*. **695**, 133560 (2019).

37. Burtscher, M. Effects of living at higher altitudes on mortality: a narrative review. *Aging Dis*. **5**, 274-80 (2013).

38. Curriero, F. C. et al. Temperature and mortality in eleven cities of the eastern United States. *Am. J. Epidemiol.* **155**, 80–7 (2002).

39. Xiao, J. et al. How much does latitude modify temperature–mortality relationship in 13 eastern US cities? *Int. J. Biometeorol.* **59**, 365-372 (2015).

40. Huang, Z. et al. Individual-level and community-level effect modifiers of the temperature-mortality relationship in 66 Chinese communities. *BMJ Open* **5**, e009172 (2015).

41. Ma, W., Chen, R. & Kan, H. Temperature-related mortality in 17 large Chinese cities: How heat and cold affect mortality in China. *Environ. Res*. **134**, 127–133 (2014).
42. Bakhtsiyarava, M. et al. Modification of temperature-related human mortality by area-level socioeconomic and demographic characteristics in Latin American cities. *Soc. Sci. Med*. **317**, 115526 (2023).
43. Martinez, B. F. et al. Geographic distribution of heat-related deaths among elderly persons: use of county-level dot maps for injury surveillance and epidemiologic research. *JAMA* **262**, 2246–50 (1989).
44. Smoyer-Tomic, K. E. & Rainham, D. G. Beating the heat: development and evaluation of a Canadian hot weather health-response plan. *Environ Health Perspect* **109**, 1241–8 (2001).
45. Ryti, N. R., Guo, Y. & Jaakkola, J. J. Global association of cold spells and adverse health effects: a systematic review and meta-analysis. *Environ. Health Persp.* **124**, 12-22 (2016).
46. Wang, J. et al. Significant effects of ecological context on urban trees' cooling efficiency. *ISPRS J. Photogramm. Remote Sens*.159, 78–89 (2020).
47. Yang, Q. et al. Global assessment of urban trees' cooling efficiency based on satellite observations. *Environ. Res. Lett.* **17**, 034029 (2022).
48. Winbourne, J. B. et al. Tree transpiration and urban temperatures: current understanding, implications, and future research directions. *Bioscience* **70**, 576–588 (2020).
49. Manoli, G. et al. Magnitude of urban heat islands largely explained by climate and population. *Nature* **573**, 55–60 (2019).
50. Zhao, L., Lee, X., Smith, B. R. & Oleson, K. Strong contributions of local

background climate to urban heat islands. *Nature* **511**, 216–219 (2014).

51. Wang, C., Wang, Z. H., Wang, C. & Myint, S. W. Environmental cooling provided by urban trees under extreme heat and cold waves in U.S. cities. *Remote Sens. Environ*. **227**, 28–43 (2019).

52. Bonafoni, S., Baldinelli, G., Rotili, A. & Verducci, P. Albedo and surface temperature relation in urban areas: Analysis with different sensors. *Joint Urban Remote Sensing Event (JURSE)* (2017).

53. Santamouris, M. Cooling the cities–a review of reflective and green roof mitigation technologies to fight heat island and improve comfort in urban environments. *Solar Energy* **103**, 682-703 (2014).

54. Iungman, T. et al. Cooling cities through urban green infrastructure: a health impact assessment of European cities. *The Lancet* **401**, 577–589 (2023).

55. Gasparrini, A. et al. Projections of temperature-related excess mortality under climate change scenario*s. Lancet Planet. Health* **1**, e360-e367 (2017).

56. Yin, Q., Wang, J., Ren, Z., Li, J. & Guo, Y. Mapping the increased minimum mortality temperatures in the context of global climate change. *Nat. Commun*. **10**, 4640 (2019).

57. Jones, B. et al. Future population exposure to US heat extremes. *Nat. Clim. Change* **5**, 652-655 (2015).

58. Lüthi, S. et al. Rapid increase in the risk of heat-related mortality. *Nat. Commun*. **14**, 4894 (2023).

59. Baldwin, J. W., Dessy, J. B., Vecchi, A. G. & Oppenheimer, M. Temporally compound heat wave events and global warming: An emerging hazard. *Earth's Future* **7**, 411–427 (2019).